

AWARD NUMBER: W81XWH-13-1-0244

TITLE:  
Identification, Characterization, and Utilization of Adult Meniscal Progenitor Cells

PRINCIPAL INVESTIGATOR: Dr. Vicki Rosen

CONTRACTING ORGANIZATION: Harvard University, Boston  
Boston, MA 02115

REPORT DATE: November 2017

TYPE OF REPORT: Final

PREPARED FOR: U.S. Army Medical Research and Materiel Command  
Fort Detrick, Maryland 21702-5012

DISTRIBUTION STATEMENT: Approved for Public Release;  
Distribution Unlimited

The views, opinions and/or findings contained in this report are those of the author(s) and should not be construed as an official Department of the Army position, policy or decision unless so designated by other documentation.

REPORT DOCUMENTATION PAGE				Form Approved OMB No. 0704-0188	
Public reporting burden for this collection of information is estimated to average 1 hour per response, including the time for reviewing instructions, searching existing data sources, gathering and maintaining the data needed, and completing and reviewing this collection of information. Send comments regarding this burden estimate or any other aspect of this collection of information, including suggestions for reducing this burden to Department of Defense, Washington Headquarters Services, Directorate for Information Operations and Reports (0704-0188), 1215 Jefferson Davis Highway, Suite 1204, Arlington, VA 22202-4302. Respondents should be aware that notwithstanding any other provision of law, no person shall be subject to any penalty for failing to comply with a collection of information if it does not display a currently valid OMB control number. <b>PLEASE DO NOT RETURN YOUR FORM TO THE ABOVE ADDRESS.</b>					
1. REPORT DATE November 2017		2. REPORT TYPE Final		3. DATES COVERED 1 Sept 2013 – 31 Aug 2017	
4. TITLE AND SUBTITLE Identification, Characterization, and Utilization of Adult Meniscal Progenitor Cells				5a. CONTRACT NUMBER	
				5b. GRANT NUMBER W81XWH-13-1-0244	
				5c. PROGRAM ELEMENT NUMBER	
6. AUTHOR(S) Vicki Rosen  E-Mail: Vicki_Rosen@hsdm.harvard.edu				5d. PROJECT NUMBER	
				5e. TASK NUMBER	
				5f. WORK UNIT NUMBER	
7. PERFORMING ORGANIZATION NAME(S) AND ADDRESS(ES) Harvard University, Boston Boston, MA 02115				8. PERFORMING ORGANIZATION REPORT NUMBER	
9. SPONSORING / MONITORING AGENCY NAME(S) AND ADDRESS(ES)  U.S. Army Medical Research and Materiel Command Fort Detrick, Maryland 21702-5012				10. SPONSOR/MONITOR'S ACRONYM(S)	
				11. SPONSOR/MONITOR'S REPORT NUMBER(S)	
12. DISTRIBUTION / AVAILABILITY STATEMENT  Approved for Public Release; Distribution Unlimited					
13. SUPPLEMENTARY NOTES					
14. ABSTRACT Meniscal injuries are the most common traumatic leg injuries, accounting for over half of the knee arthroscopies performed each year. Damaged menisci rarely regain normal structural integrity or mechanical strength, and surgical repair cannot reliably prevent the degenerative changes that occur post injury and presage the development of knee osteoarthritis (OA). New treatments centered on the stem/progenitor cell population resident within the adult meniscus will be key to derailing the connection between acute meniscal injury and post-traumatic knee OA. Here we combine mouse genetics with molecular and cell biology to develop a profile of repair cells in the adult meniscus, track meniscal stem/progenitor cell (MSPC) behavior within meniscus as function of age, and assess the contribution of resident MSPCs to repair after meniscal injury. During the research period we made significant progress toward our goals by establishing a standard protocol for harvesting MSPCs from 8 week, 6 month and 1-year old mouse menisci. MSPCs grow as colonies, express stem cell and meniscal gene signature markers found in adult human meniscus, and can be successfully passaged. We also piloted a novel mouse meniscal tear injury model, and are now ready to use this technique to examine the role of meniscal stem cells in injury repair.					
15. SUBJECT TERMS meniscus, meniscal cells, stem cells, progenitor cells, meniscus healing, meniscus repair, osteoarthritis					
16. SECURITY CLASSIFICATION OF:			17. LIMITATION OF ABSTRACT	18. NUMBER OF PAGES	19a. NAME OF RESPONSIBLE PERSON
a. REPORT	b. ABSTRACT	c. THIS PAGE			USAMRMC
Unclassified	Unclassified	Unclassified	Unclassified	43	19b. TELEPHONE NUMBER (include area code)

## Table of Contents

	<u>Page</u>
1. Introduction.....	4
2. Keywords.....	4
3. Overall Project Summary.....	4
4. Key Research Accomplishments .....	8
5. Conclusion.....	9
6. Publications, Abstracts and Presentations.....	9
7. Inventions, Patents and Licenses.....	10
8. Reportable Outcomes.....	10
9. Other Achievements.....	10
10. References.....	10
11. Appendices.....	11

## **1. Introduction**

Meniscal injuries are the most common of traumatic knee injuries (1,2). Once damaged, meniscal tissue rarely regains normal structural integrity and mechanical strength (3,4). Surgical repair of meniscal tears cannot reliably prevent the degenerative changes that occur after injury (5,6). As a result, meniscal injuries are a common underlying cause of post-traumatic osteoarthritis. This is particularly striking in young, healthy individuals such as military personnel, where meniscal injury is often associated with long-term disability and knee replacement surgery (7,8). This proposal focuses on identifying meniscal stem/progenitor cells (MSPC) in the adult meniscus, developing a molecular profile of these cells, and examining the contribution MSPC provide to repair after meniscal injury. Information gathered from these studies will be useful for developing new treatments for acute meniscal injuries, lessening the need for joint replacement and reducing long-term disability in active adults.

## **2. Keywords**

meniscus, meniscal cells, stem cells, progenitor cells, meniscus healing, meniscus repair, osteoarthritis

## **3. Overall Project Summary**

### **1. Isolation and characterization of MSPC.**

**Task 1:** Obtain mice necessary for experiments. This task has been completed.

**Task 2:** Develop standard MSPC isolation protocol. This task has been completed and published in Gamer et al., 2017.

**Task 3:** Characterize MSPC.

**Subtasks (3a-3d)** have been completed and published in Gamer et al., 2017.

**Subtask (3e):** Self-renewal capacity of MSPCs will be examined by calculating proliferation rates using a BrdU assay, and doubling times will be determined. This task has not been completed.

**Subtask (3f):** Migratory capacity of MSPCs will be determined and test substances IGF1, BMP2, and TGF $\beta$  evaluated. This task has not been completed.

## **2. Interaction of MSPC with meniscus niche in vivo.**

**Task 1:** Obtain and age mice for experiments. This task has been completed.

**Task 2:** Introduce MSPC into meniscus in vivo.

We have experienced difficulty in injecting meniscal cells into the mouse meniscus. The small size and accessibility of the mouse knee has been a challenge. Due to these issues, this task has not been completed.

**Task 3:** Track MSPC behavior. This has not yet been attempted due to difficulties with Task 2.

**Task 4:** Analyze MSPC niche in adult meniscus. Data have been collected in young mice and published in Gamer et al., 2017.

**Task 5:** Assess functional changes in meniscus due to addition of MSPC. These studies have not been started.

**Task 6:** Assess effects of niche age on MSPC. These studies have not been started.

**3. Functional assessment of healing by MSPC.**  
**Task 1:** Obtain mice for experiments:  
Mice are available for these studies.

**Task 2:** Introduction of MSPC into adult meniscus. This task has not yet been attempted due to the difficulties outlined above with injection of MSPCs into mouse meniscus in vivo.

**Task 3:** Production of meniscus tear.

No model exists to study acute meniscal injury in the mouse so it has not been possible to assess signaling and cellular changes within the meniscus immediately after injury or monitor the temporal contribution of injured meniscus to the joint environment. To address this problem, we created a simple meniscus injury model (Fig 1). We note that the exact injury made by this procedure varies (Fig 1C), similar to the highly variable injuries that occur in individuals after meniscus trauma.

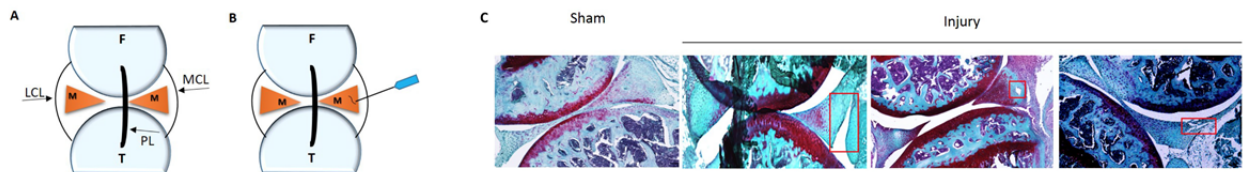


Fig 1: Meniscus injury model . (A) A small skin incision is made above the left knee. The patella ligament (PL) is identified and carefully moved aside. (B) A 25G needle is inserted inside the knee just in front the medial collateral ligament (MCL) and quickly removed. The skin is sutured and mice are allowed to ambulate freely. F-Femur. T-Tibia. (C) Injuries vary from (L-R) longitudinal tear, puncture, or horizontal tear.

**Task 4:** Tracking MSPC participation in repair. This task has not yet been attempted as the meniscus tear model is still being assessed.

**Task 5:** Analysis of repair process.

The data shown in Fig 2 was obtained from n=6 mice per time point; all had biological responses to injury even if the injury type varied. Meniscal tear injury activates cells resident in adult meniscus. When we localized cell proliferation after injury using Ki67 expression, we observed a small increase in proliferating cells at 3 days after injury and a substantial increase in proliferating cells 21 days after injury (Fig 2B). This response is consistent with the idea that meniscal progenitors are maintained in a quiescent state and

are mobilized after injury in response to signaling changes. Meniscal tear injury leads to up regulation of MMP13 in meniscus and articular cartilage. We followed the changes in the knee joint after acute meniscus injury using histology and IHC. The most striking changes we observed were on day 21 after surgery, when both the meniscus and the adjacent articular cartilage expressed MMP13 (Fig 3C), a finding highly relevant for understanding the progression of events within the knee after acute meniscus injury as proteolytic cleavage of aggrecan by MMP13 weakens extracellular matrix (ECM) and is a key element in the pathogenesis of OA. Models of meniscus injury in larger animals have established that injured meniscus is a source of activated MMPs, and in some of these studies inhibiting MMP13 activity has protective effects, slowing the progression of joint disease. MMP13 is reported to be expressed in cartilage of human OA patients and not present in normal adult cartilage. Examining gene expression in human meniscal samples early after injury is difficult because joint replacement surgery is not performed early after meniscus injury and data from knees at time of joint replacement has been highly variable with regard to gene expression by meniscus. While surgery is performed to repair meniscus after tearing has occurred, meniscus tissue is usually not harvested during these procedures. Availability of a mouse model allows us to address the issue of meniscus gene expression as a function of time after injury, and more generally to test our hypothesis for why the meniscus does not repair after injury.

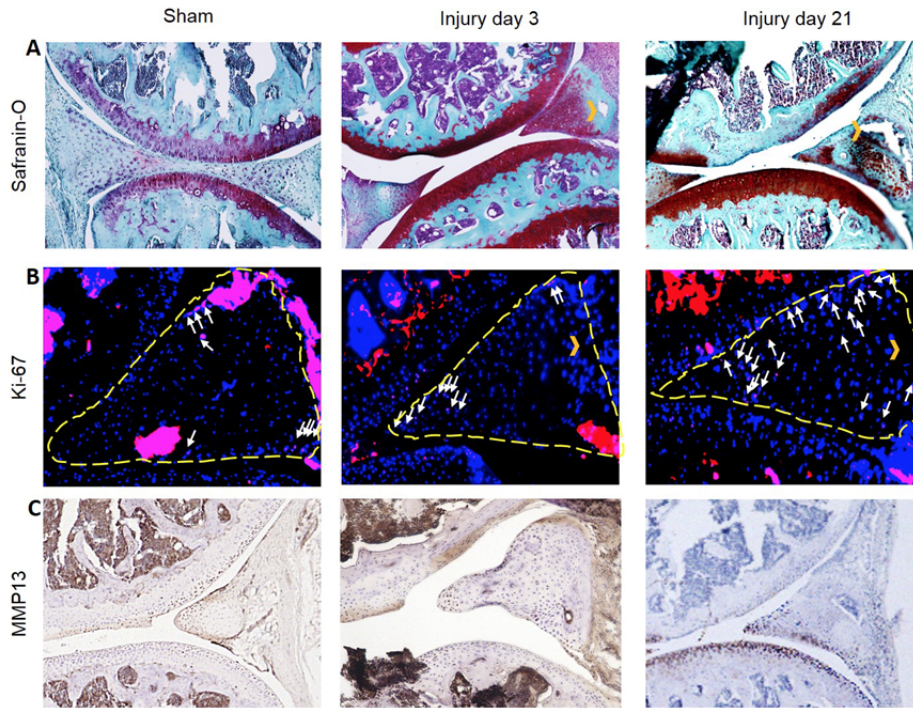


Fig 2: Evaluation of meniscus injury . Knees harvested at d3 and d21 after surgery. A. Safranin O (Saf O): 10x mag B. IF for Ki67 20x mag Blue = DAPI. Red = Ki67. C. IHC for MMP13. 10x mag D. Meniscus cells harvested 3 hours after injury were assessed for CFU-F. Section thickness = 10um.

**Task 6:** Effect of enhancing signaling on repair. This task has not yet been attempted.

**Task 7:** Effect of adding exogenous MSPC on repair. This task has not yet been attempted.

#### **4. Key Research Accomplishments**

1. Development of reproducible and efficient protocol for isolation of meniscal stem/progenitor cells (MSPC) from adult mouse meniscus.
2. Characterization of stem cell features of MSPC from young and aged mice.
3. Development of reproducible meniscal tear model in adult mice.
4. Characterization of endogenous healing capacity in meniscal tear model in adult mice.



## **5. Conclusion**

Treatment options for damaged meniscus are limited and all have a poor outcome when judged by their ability to prevent progression of degenerative changes within the meniscus and adjacent articular cartilage so that meniscus damage remains a potent risk factor for knee OA. Availability of mouse models has greatly enhanced our knowledge of the mechanisms underlying the repair of musculoskeletal tissues as murine models exhibit similar pathological characteristics as humans (9). Prior to completing this project, no characterization of MSPC from adult mice had been reported, nor had a mouse model of meniscal injury been developed. As a result, we have not been able to study the signaling changes and cellular events that take place within the meniscus immediately after injury or monitor the temporal contribution of injured meniscus to the increasingly destructive joint environment that develops and negatively affects other tissues within the joint space. Availability of these novel reagents will allow us to map the biological events that culminate in post-traumatic knee OA, assessing the injured meniscus first, and following subsequent changes in other joint tissues that occur in response to meniscal injury. These investigations will provide a new perspective on the relationship between the pathogenic events that define OA. Insight garnered from a mouse model of meniscal injury will also help define design principles for novel meniscal replacements, an area where current progress in developing enhanced grafting materials is limited by lack of information regarding the origin of meniscal progenitor cells and the signals controlling their differentiation and proliferation, areas we can easily investigate due to our characterization of MSPC (10).

## **6. Publications, Abstracts and Presentations**

### **a. Journal publications:**

Muhammad H, Schminke B, Bode C, Roth M, Albert J, von der Heyde S, **Rosen V** and Miosge N. Human Migratory Meniscus Progenitor Cells Are Controlled via the TGF- $\beta$  Pathway. *Stem Cell Reports*, 2014 Nov 11; 3(5): 789–803. PMID 25418724.

Li Q, Doyran B, Gamer L, Lu X, Qin L, Ortiz C, Grodzinsky A, **Rosen V**, Han L. Biomechanical properties of murine meniscus surface via AFM-based nanoindentation. *J Biomech*. 2015; 48:1364-1370; PMID: 25817332.

Gamer LW, Shi RR, Gendelman A, Mathewson D, Gamer J, **Rosen V**. Identification and characterization of adult mouse meniscus stem/progenitor cells. *Connect Tissue Res*. 58(3-4): 238-245 (2017). PMID: 28005443.

**b. Other publications, conference papers and presentations:**

Isolation and Characterization of Adult Mouse Meniscus Stem/Progenitor Cells. Gamer LW, Shi R, Gendelman A, Mathewson D, Gamer J, **Rosen V**. Abstract presented at Orthopaedic Research Society meeting, San Diego, CA, March 19-22, 2017.

Developing a Novel Model for Studying Meniscus Injury. Feigenson M, Gamer LW, **Rosen V**. Abstract submitted to Orthopaedic Research Society meeting, New Orleans, LA, March 10-13, 2018.

**7. Inventions, Patents and Licenses.** Nothing to report.

**8. Reportable Outcomes**

1. Development of reproducible and efficient protocol for isolation of meniscal stem/progenitor cells (MSPC) from adult mouse meniscus.
2. Characterization of stem cell features of MSPC from young and aged mice.
3. Development of reproducible meniscal tear model in adult mice.
4. Characterization of endogenous healing capacity in meniscal tear model in adult mice.

**9. Other Achievements.** Nothing to report.

**10. References**

1. Lohmander LS, Englund PM, Dahl LL, Roos EM. The long-term consequence of anterior cruciate ligament and meniscus injuries: osteoarthritis. *Am J Sports Med*. 2007;35(10):1756-69.
2. Englund M, Guermazi A, Lohmander LS. The meniscus in knee osteoarthritis. *Rheum Dis Clin North Am*. 2009;35(3):579-90.
3. Pabbruwe MB, Kafienah W, Tarlton JF, Mistry S, Fox DJ, Hollander AP. Repair of meniscal cartilage white zone tears using a stem cell/collagen-scaffold implant. *Biomaterials*. 2010;31(9):2583-91.

4. Starke C, Kopf S, Petersen W, Becker R. Meniscal repair. *Arthroscopy*. 2009;25(9):1033-44.
5. Myers ER, Blumrick R, Christian AL, Santanu Datta S, Gray RN, Kolimaga JT, et al. Management of prolonged pregnancy. *Evid Rep Technol Assess (Summ)*. 2002(53):1-6.
6. von Lewinski G, Kohn D, Wirth CJ, Lazovic D. The influence of nonanatomical insertion and incongruence of meniscal transplants on the articular cartilage in an ovine model. *Am J Sports Med*. 2008;36(5):841-50.
7. Deshpande BR, Katz JN, Solomon DH, Yelin EH, Hunter DJ, Messier SP, et al. Number of Persons With Symptomatic Knee Osteoarthritis in the US: Impact of Race and Ethnicity, Age, Sex, and Obesity. *Arthritis Care Res (Hoboken)*. 2016;68(12):1743-50.
8. Losina E, Paltiel AD, Weinstein AM, Yelin E, Hunter DJ, Chen SP, et al. Lifetime medical costs of knee osteoarthritis management in the United States: impact of extending indications for total knee arthroplasty. *Arthritis Care Res (Hoboken)*. 2015;67(2):203-15.
9. Moon PM, Penuela S, Barr K, Khan S, Pin CL, Welch I, et al. Deletion of Panx3 Prevents the Development of Surgically Induced Osteoarthritis. *J Mol Med (Berl)*. 2015;93(8):845-56.
10. Pena A. How Mexican biochemistry developed and present challenges. *IUBMB Life*. 2011;63(10):784-8.

## **11. Appendices**

Muhammad H, Schminke B, Bode C, Roth M, Albert J, von der Heyde S, **Rosen V** and Miosge N. Human Migratory Meniscus Progenitor Cells Are Controlled via the TGF- $\beta$  Pathway. *Stem Cell Reports*, 2014 Nov 11; 3(5): 789–803. PMID 25418724.

Li Q, Doyran B, Gamer L, Lu X, Qin L, Ortiz C, Grodzinsky A, **Rosen V**, Han L. Biomechanical properties of murine meniscus surface via AFM-based nanoindentation. *J Biomech*. 2015; 48:1364-1370; PMID: 25817332.

Gamer LW, Shi RR, Gendelman A, Mathewson D, Gamer J, **Rosen V**. Identification and characterization of adult mouse meniscus stem/progenitor cells. *Connect Tissue Res*. 58(3-4): 238-245 (2017). PMID: 28005443.

Isolation and Characterization of Adult Mouse Meniscus Stem/Progenitor Cells. Gamer LW, Shi R, Gendelman A, Mathewson D, Gamer J, **Rosen V**. Abstract presented at Orthopaedic Research Society meeting, San Diego, CA, March 19-22, 2017.

List of Personnel supported on this Project.



# Human Migratory Meniscus Progenitor Cells Are Controlled via the TGF- $\beta$ Pathway

Hayat Muhammad,<sup>1,4</sup> Boris Schminke,<sup>1,4</sup> Christa Bode,<sup>1</sup> Moritz Roth,<sup>1</sup> Julius Albert,<sup>1</sup> Silvia von der Heyde,<sup>2</sup> Vicki Rosen,<sup>3</sup> and Nicolai Miosge<sup>1,\*</sup>

<sup>1</sup>Tissue Regeneration Work Group, Department of Prosthodontics, Medical Faculty, Georg-August-University, 37075 Goettingen, Germany

<sup>2</sup>Institute of Medical Statistics, Medical Faculty, Georg-August-University, 37075 Goettingen, Germany

<sup>3</sup>Developmental Biology, Harvard School of Dental Medicine, Boston, MA 02115, USA

<sup>4</sup>Co-first author

\*Correspondence: [nmiosge@gwdg.de](mailto:nmiosge@gwdg.de)

<http://dx.doi.org/10.1016/j.stemcr.2014.08.010>

This is an open access article under the CC BY-NC-ND license (<http://creativecommons.org/licenses/by-nc-nd/3.0/>).

## SUMMARY

Degeneration of the knee joint during osteoarthritis often begins with meniscal lesions. Meniscectomy, previously performed extensively after meniscal injury, is now obsolete because of the inevitable osteoarthritis that occurs following this procedure. Clinically, meniscus self-renewal is well documented as long as the outer, vascularized meniscal ring remains intact. In contrast, regeneration of the inner, avascular meniscus does not occur. Here, we show that cartilage tissue harvested from the avascular inner human meniscus during the late stages of osteoarthritis harbors a unique progenitor cell population. These meniscus progenitor cells (MPCs) are clonogenic and multipotent and exhibit migratory activity. We also determined that MPCs are likely to be controlled by canonical transforming growth factor  $\beta$  (TGF- $\beta$ ) signaling that leads to an increase in SOX9 and a decrease in RUNX2, thereby enhancing the chondrogenic potential of MPC. Therefore, our work is relevant for the development of novel cell biological, regenerative therapies for meniscus repair.

## INTRODUCTION

In the elderly, osteoarthritis (OA) is the most common musculoskeletal disease (Reginster, 2002) and will be the fourth leading cause of disability by the year 2020 (Woolf and Pfleger, 2003). The knee is particularly prone to meniscal lesions that lead to OA (Englund et al., 2012), and a high interdependency of OA and meniscus lesions has been described (Brophy et al., 2012). In fact, meniscal injuries are the most common knee injury and account for more than 50% of the 1.5 million knee arthroscopies performed annually (Englund et al., 2008; Lohmander et al., 2007). The prevalence of meniscal tears increases with age (Loeser, 2013) and may be as high as 56% in men aged 70–90 years old (Englund et al., 2008). Lack of robust meniscal repair in adults with or without surgical intervention has led to the development of allografts or bioengineered meniscal substitutes (Haddad et al., 2013; Steinert et al., 2007), and, whereas these fill the space void created following removal of the meniscus, clinical, radiological, and MRI evaluations show no protection against the development of OA (Homen et al., 2007). The specific reasons for this lack of effect are unknown; however, a failure to successfully remodel the allograft into living tissue is one likely factor (Steadman and Rodkey, 2005). Almost all patients eventually require joint replacement (Lohmander and Roos, 2007).

The meniscus is best described as a fibrocartilage (Benjamin and Evans, 1990) comprising an outer, “red vascularized” part and an inner “white, unvascularized” part harboring round fibrochondrocytes (Hellio Le Graverand

et al., 2001). Additionally, the outer surface of the meniscus is enclosed by a superficial layer with flattened, elongated fibroblast-like cells that predominantly synthesize collagen type I (McDevitt and Webber, 1990), whereas the round fibrochondrocytes from the inner part also produce collagen type II (Chevrier et al., 2009).

It has long been known that the outer, vascularized part of the meniscus is often able to successfully repair itself after injury allowing for normal meniscus function, whereas the inner meniscus produces a repair tissue in response to injury but cannot functionally regenerate. Experimental animal studies support the idea that the meniscus possesses regeneration activity. For example, fibrochondrocytes have been isolated from bovine meniscus tissue (Mauck et al., 2007) and migrating cells are found in healthy adult rabbit meniscus (Webber et al., 1989). Regeneration of the vascular, outer part of the meniscus might be due to the presence of CD34-positive cells (Osawa et al., 2013) or to mesenchymal cells that can be released by collagenase digestion of human meniscus (Segawa et al., 2009). Because application of growth factors and fibrin clots have elicited responses by cells resident in the inner meniscus, several authors have speculated about the importance of activation of meniscal repair cells (Petersen et al., 2005). Up until today, the question remains, as to whether the inner, avascular part of the human meniscus harbors multipotent cells capable of regeneration.

Here, we describe isolation of human meniscus progenitor cells (MPCs) from the inner meniscus harvested from

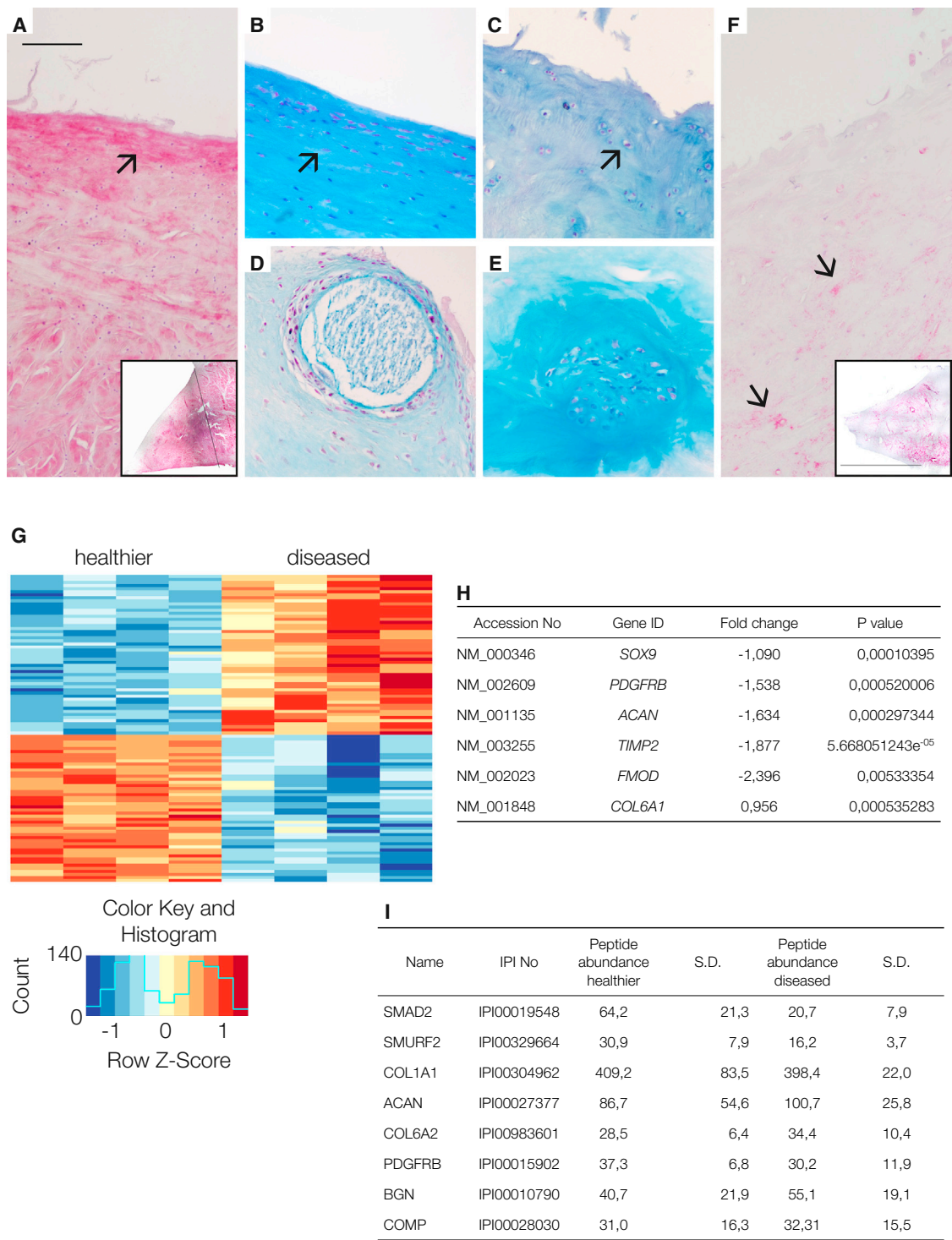


**Figure 1. Characterization of Human Healthy and Diseased Meniscus Tissue**  
(A) Immunohistochemistry of collagen type I in healthier meniscus (arrow); inset: low magnification of a human healthier meniscus stained for collagen type I; the black line indicates the border between the vascular part on the right side and the avascular part on the left side.  
(B) Healthier human meniscus with an intact superficial zone and flattened cells (arrow).  
(C) Diseased meniscus with a completely degenerated superficial zone where only the round cells of the inner zone remain (arrow).

(legend continued on next page)



late-stage OA patients prior to knee replacement and show that the regenerative potential of these cells is governed by transforming growth factor  $\beta$  (TGF- $\beta$ ) signaling.

## RESULTS

### Meniscus Tissue Histology and Molecular Composition

By combining and modifying available classification systems for OA specimens (Pauli et al., 2011; Zhang et al., 2011), we developed a means to discriminate healthier human menisci from their diseased counterparts. Intact meniscus tissue is composed of a superficial zone with flattened cells that primarily synthesize collagen type I (McDevitt and Webber, 1990). This architecture remains in healthier human menisci obtained from patients suffering from OA but is always absent in more disease samples (Figures 1A and 1B). The inner zone, containing more rounded cells that secrete collagen type I and type II, is present regardless of disease severity (Figures 1C and 1F). In diseased human menisci (score greater 4), 23% of the samples exhibit abnormal calcifications (Figure 1D) and 53% display anomalous clusters of cells (Figure 1E).

Using microarrays, we then analyzed cells obtained by culturing tissue explants from the inner zone of diseased and healthier human menisci. We focused on the top 100 most abundantly expressed genes, and among these, we identified 48 as being upregulated, i.e., exhibiting a positive fold change, and 52 as being downregulated, i.e., exhibiting a negative fold change ( $p$  value  $<0.001$ , as listed in the figure legend). Among these top 100 genes, we found only four of the 15 arbitrarily defined potential marker genes: TIMP2, SOX9, ACAN, and MMP14, stressing the

importance of these particular genes for discriminating healthier meniscal samples from diseased ones. When we analyzed eight human meniscus tissue samples, the 100 top genes clustered into two groups, healthier and diseased, as shown in the heatmap (Figure 1G). A selection is listed (Figure 1H), and the complete results can be found under GEO (accession number GSE52042).

To complement our microarray analyses, we performed proteomics analyses on cells grown from the healthier and diseased meniscus samples and could identify approximately 4,000 proteins as expressed by meniscal explant cells. However, only a small number of proteins produced by meniscal cells are known to be relevant for OA and meniscus pathology (as listed in Figure 1I), suggesting that for the meniscus, like other tissues studied so far, the correlation between transcriptome and proteome data is weak (Haider and Pal, 2013). Upon close examination, several signaling pathway mediators stood out as being differentially expressed between cells from healthier and diseased meniscal samples. In particular, SMAD2, a mediator of the canonical TGF- $\beta$ /activin signaling pathway was more abundant in healthier meniscus cells (Figure 1I; for a full listing, visit <http://www.miosge.med.uni-goettingen.de/de/?id=17>). To follow up on this finding, we performed immunohistochemical (IHC) staining and found that meniscus samples that received a high disease score exhibited a reduced IHC staining for TGF- $\beta$  and SMAD2. Consistent with these findings, proteome analysis and western blotting of diseased specimens also showed a reduction in SMAD2 protein and an upregulation of RUNX2 compared to healthier specimens. These results, together with existing literature, indicated that the TGF- $\beta$ /BMP pathway, with its dual osteogenic and chondrogenic actions (Massagué, 2012), was a good candidate to investigate in greater detail.

(D and E) Calcifications (D) and cell clusters (E) are signs of OA.

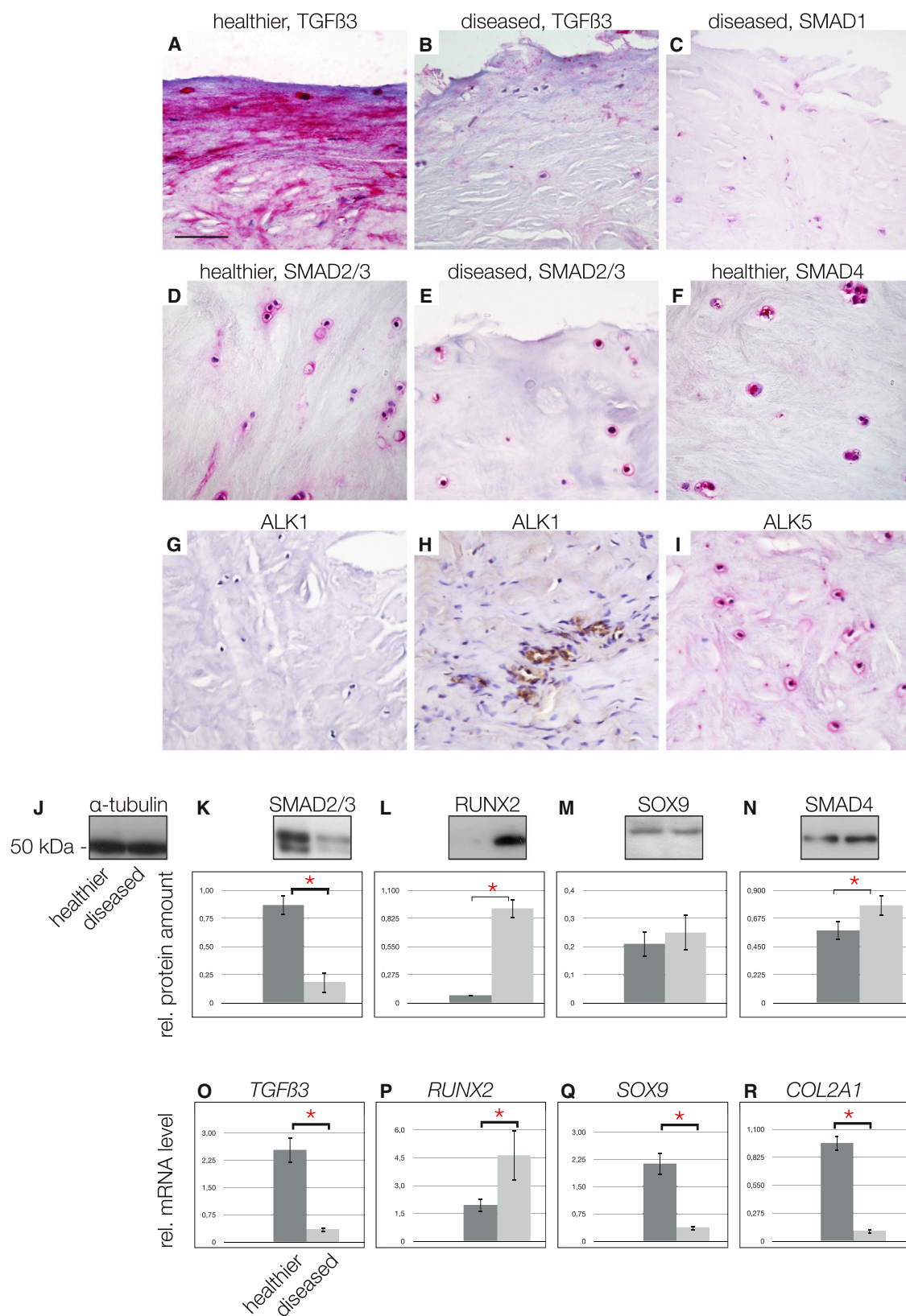
(F) Immunohistochemistry of collagen type II in diseased meniscus (arrows); inset: low magnification of a human diseased meniscus stained for collagen type II. Magnification in (A)–(F), scale bar, 150  $\mu$ m; inset bar, 1.7 cm.

(G) Heatmap of the top 100 differentially expressed genes with  $p$  values  $<0.001$ . The red color indicates upregulated genes, and the blue color indicates downregulated genes. The upregulated genes in diseased meniscus compared with healthier tissue are ACTR2, KRT, HSPD1, CALU, HSPA9, BAX, CCDC80, C17orf59, HSP90AB1, CDC42, HNRNP1, FKBP9, MT1DP, G3BP1, CTTN, COL6A1, TAF15, ELAVL1, MCL1, AL, HSPA4, CXorf40A, CXorf40B, TCP1, RP5, VHL, PRPF4, BAG5, RIOK3, FCF1, SPTLC1, APH1A, RNF170, RCN3, DENR, CAPZB, MBNL1, CASC4, ASB1, MRPS10, RAB23, PAAF1, FARSB, NASP, NUDC, ZNF346, RIOK1, and GAR1. The downregulated genes in diseased meniscus compared with healthier tissue are RNF103, SLC41A3, SNX19, GTIFP1, ERF, NBPF10, NBPF3, OSBPL10, ADAM15, KIAA0930, ZMAT3, AL845464.3, ANTXR1, ENDOD1, ZNFX1, GLT8D2, RP5-1022P6.4, ENG, POMZP3, C11orf95, LPCAT1, EPN2, POMZP3, RAB11FIP3, TBC1D2B, PCDHGC3, MMP14, TRPM4, HDAC5, ABL1, SOX9, Antxr1, BCAN, ZP3, ABR, SNX33, RPS6KA4, CXCR7, NCOR2, PLEC, GPC1, SEMA3C, PDGFRB, LUM, ACAN, CSPG4, OAS1, TIMP2, VCAM1, LAM5, PRSS54, PCDHB1, and FMOD.

(H) Selected microarray data of genes that are known from the literature to be highly expressed in healthy hyaline cartilage tissue (SOX9, PDGFRB, ACAN, TIMP2, and FMOD). These genes were significantly downregulated in cells derived from diseased tissue compared with cells from healthier meniscus tissue. Only COL6, as indicator gene of an active pericellular matrix of chondrocytes (Poole et al., 1992), is upregulated.

(I) Peptide abundance of selected genes shown as the mean of four experiments that analyzed cells that migrated out from meniscus from healthier and diseased samples in vitro (SD).





(legend on next page)

**Table 1. Primer Sequences**

GeneID	Forward Primer	Reverse Primer	Accession Number
<i>SMAD1</i>	5'-TCTTCAGAGCCACCATGAATAA-3'	5'-AACCAGCACAGGAGGAAGTACAG-3'	NM_005900
<i>SMAD2</i>	5'-GTCTCTTGATGGTCGTCTCCA-3'	5'-TTCTGTTAGGATCTCGGTGTGTC-3'	NG_029946
<i>SMAD3</i>	5'-CCATCCTGCCTTCACTC-3'	5'-TGGTGATGCACTTGGTGT-3'	AB004922
<i>SMAD4</i>	5'-GCACAAGGTGGTTGCTAAGA-3'	5'-GCAGAACAGTGAGACATTAGGTAGAG-3'	NG_013013
<i>TGF-β3</i>	5'-CTTTGGACCAATTACTGCTTC-3'	5'-GGGTTCAAGTGTGTACAGTCC-3'	NM_003239.2
<i>RUNX2</i>	5'-TTCAGACCAGCAGCACTC-3'	5'-CAGCGTCAACACCATCATT-3'	NM_004348
<i>COL1A1</i>	5'-TTCCCCAGCCACAAGAGTC-3'	5'-CGTCATCGACAACACCT-3'	NM_000088
<i>COL2A1</i>	5'-CTCCTGGAGCATCTGGAGAC-3'	5'-ACCACGATCACCTTGACTC-3'	NM_033150
<i>SOX9</i>	5'-CAGGCTTGCATTAAAGGA-3'	5'-CCGTTTAAAGGCTCAAGGTG-3'	Z46629
<i>β2M</i>	5'-TGCTGTCTCCATGTTGATGATCT-3'	5'-TCTCTGCTCCCACTCTAA-3'	NM_004048

### TGF-β/BMP Signaling in Human Osteoarthritic Meniscus Tissue

Because the deregulation of TGF-β family proteins has been described to be important for meniscus pathology (de Mulder et al., 2013), we examined the TGF-β status of our samples. We observed greater staining for TGF-β3 in healthier (Figure 2A) tissue compared with diseased (Figure 2B) human menisci and also found more SMAD2/3 staining in healthier tissue (Figure 2D). Reduced staining for SMAD1 was also observed in diseased tissue (Figure 2C) compared with healthier specimens (data not shown). SMAD4 staining appeared to be similar between the two groups of human menisci (Figure 2F; data not shown). When we examined the tissues for the presence of TGF-β receptors, we did not find ALK1 expression in healthier meniscus tissues (Figure 2G) but did observe staining in blood vessels of the outer vascularized part of the same specimen, consistent with reported expression of ALK1 in endothelial cells (Figure 2H; Goumans et al., 2003). How-

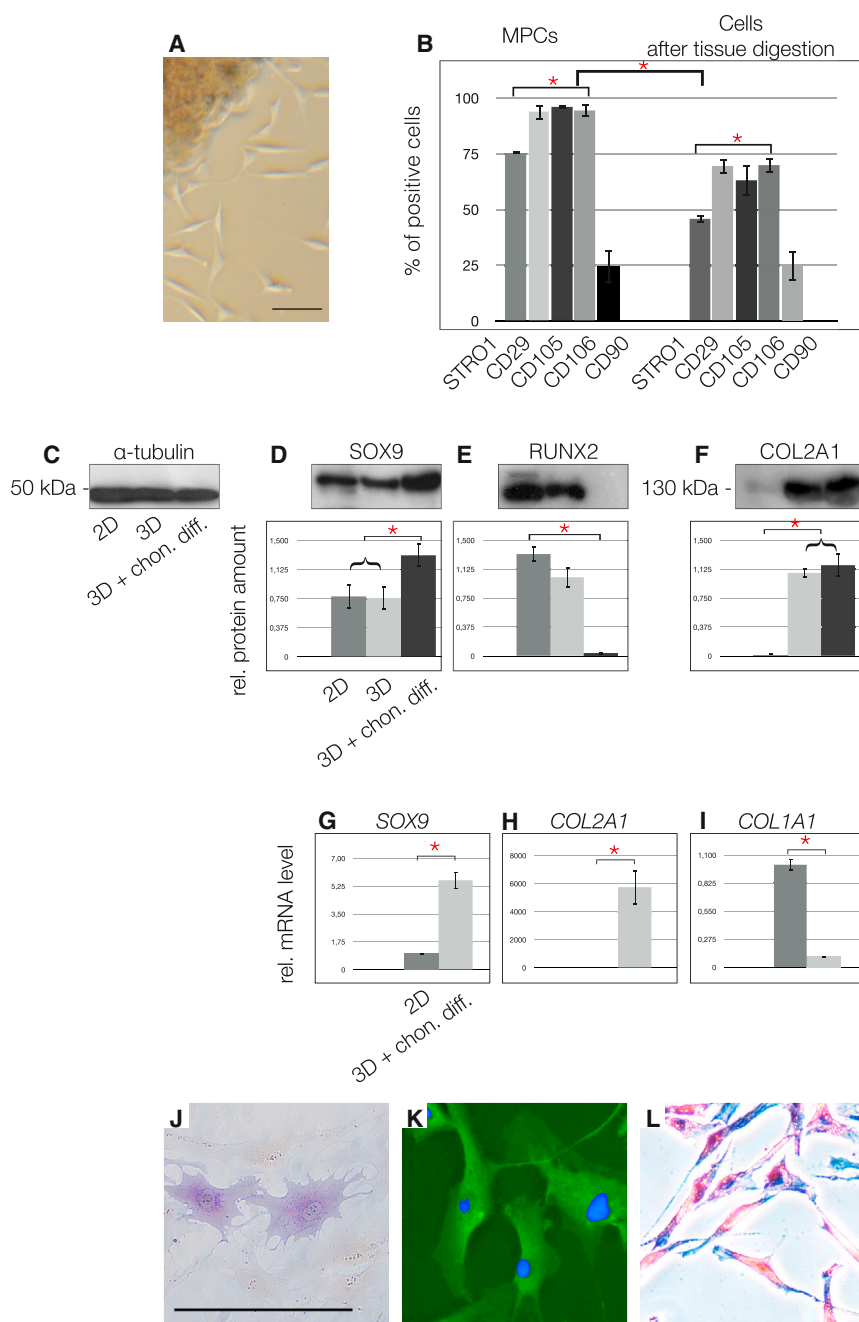
ever, staining for ALK5 was positive in the healthier meniscus (Figure 2I). Some of our IHC findings were verified by western blotting using tissue extracts from the inner zone of the menisci. All blots were quantified using ImageJ64 with α-tubulin used as a control (Figure 2J). A significantly higher level of SMAD2/3 was detected in healthier than in diseased tissue extracts (Figure 2K). Interestingly, we found greater level of RUNX2 and SMAD4 in diseased specimens (Figures 2L and 2N), whereas SOX9 levels were not altered significantly (Figure 2M). Real-time RT-PCR (for primer sequences, see Table 1) revealed results consistent with western blotting for the expression of TGF-β3 (Figure 2O) and RUNX2 (Figure 2P). Expression of SOX9 mRNA was reduced in diseased specimens (Figure 2Q), as was the expression of collagen type II (Figure 2R). Why the SOX9 mRNA reduction is not seen on the protein level remains unclear but may be due to the half-life of the protein. The simultaneous reduction in TGF-β3 and SMAD2/3 and greater levels of RUNX2 seen

### Figure 2. The TGF-β Pathway Players in Healthy and Diseased Meniscus Tissue

(A and B) Healthier meniscus stained for TGF-β3 (A) compared with the sparse staining in diseased meniscus (B). (C–E) Sparse staining of SMAD1 in diseased meniscus tissue (C). SMAD2/3 in healthier (D) compared to diseased meniscus tissue (E). (F–H) SMAD4 staining in healthier meniscus tissue (F). No ALK1 staining was detectable in healthier meniscus tissue (G), whereas blood vessels from the outer, vascularized part of the same specimen served as positive control (H). (I) However, ALK5 was detected in healthier meniscus tissue. Magnification in (A)–(I); scale bar, 150 μm. (J–N) Western blotting and quantification using ImageJ64: (J) α-tubulin shows equal loading; the first lanes of the blots corresponding to the dark gray bars in the graphs always show the healthier specimens. The diseased specimens are always found in the second lanes of the blots, which correspond to the light gray bars in the graphs. A significantly greater level of SMAD2/3 in healthier meniscus tissues is found (K). RUNX2 is almost undetectable in healthier tissue, whereas it is significantly elevated in diseased meniscus (L). SOX9 showed no significant differences between tissue types (M). SMAD4 was increased significantly in diseased meniscus (N). (O–R) Quantitative real-time RT-PCR results: (O) *TGF-β3* mRNA is significantly increased in healthier meniscus tissue; however, *RUNX2* mRNA levels are significantly reduced in healthier meniscus (P). (Q and R) (Q) *SOX9* mRNA is significantly reduced in diseased meniscus, which is in line with the significant reduction in collagen type II mRNA (R).

\*Significant differences ( $p \leq 0.05$ ); error bars denote the means  $\pm$  SD of three different healthier and three different diseased samples of OA patients for mRNA and western blotting experiments.





in diseased meniscus have been identified as a hallmark of osteochondroprogenitor cells that are present in human tissue at late stages of OA (Koelling et al., 2009; Seol et al., 2012) and suggested to us that diseased meniscus may also contain an increased number of progenitor cells.

#### Cells from Diseased Human Meniscus In Vitro Are Similar to the Cells Found In Vivo

We used explant cultures of diseased human meniscus from late-stage OA to further examine the resident osteo-

chondroprogenitor cell population. Because most OA cases are identified at late disease stages when the superficial zone of the meniscus has been completely lost, we concentrated on the cells from the inner, “white,” avascular zone. In culture, these cells grow clonally and exhibit the spindle shape typical of mesenchymal stem cells (MSCs) (Figure 3A). Consistent with this observation, fluorescence-activated cell sorting (FACS) analysis for the stem cell markers STRO1, CD29, CD90, CD105, and CD106 showed significantly higher levels of these

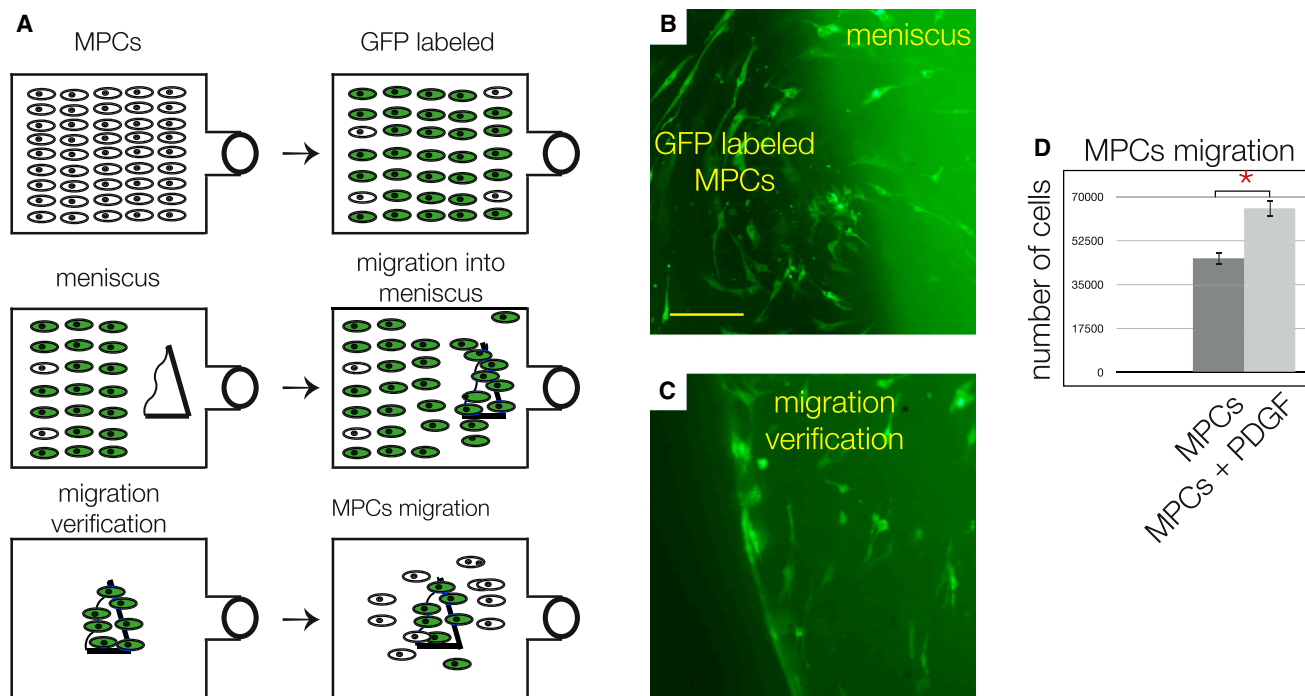


**Figure 4. Migration Potential of MPCs**

(A, top flasks) MPCs were GFP labeled, enriched via FACS to 97%, and cultured. (Middle flasks) Upon reaching 80% confluence, one side was scraped, and a sample of diseased meniscus tissue was placed on the cell-free side. After 3–4 days, MPCs repopulated and migrated into the tissue sample. (Bottom flasks) The tissues were washed with  $1 \times$  PBS solution and transferred into a new flask, and, after 7–10 days, some labeled and unlabeled MPCs migrated out again.

(B) The labeled cells adjacent to the diseased meniscus tissue.

(C) Labeled MPCs in the sample of the diseased tissue after washing and transferal to a new flask. Scale bar, 150  $\mu$ m in (C) and (D).

(D) Boyden chamber assay results showing that significantly more MPCs were attracted by human recombinant PDGF compared with controls.

\*Significant differences ( $p \leq 0.05$ ); error bars denote the means  $\pm$  SD of three individual experiments.

antigens on cells migrating out of the inner zone of diseased meniscus than in cells released after collagenase digestion of healthier specimens where the superficial zone remained intact (Figure 3B). Both populations were negative for the hematopoietic markers CD45 and CD34 (data not shown). When driven toward the chondrogenic lineage (3D alginate culture with standard chondrocyte differentiation medium) cells from damaged menisci showed 60% more SOX9 (Figure 3D), but RUNX2 was no longer detected (Figure 3E). Collagen type II appeared in chondrogenic culture conditions; however, it was undetectable in undifferentiated cells in 2D culture (Figure 3F). The levels of SOX9 (Figure 3G) and collagen type II mRNA (Figure 3H) were also significantly increased when cells were grown in 3D and chondrocyte differentiation medium. In contrast, the levels of collagen type I mRNA decreased (Figure 3I). Following osteogenic differentiation, a proportion of cells became positive for alkaline phosphatase (Figure 3J) and osteocalcin (Fig-

ure 3K), as well as alizarin red (data not shown). Oil red O-positive (Figure 3L) and PPAR $\gamma$ -positive (data not shown) adipocytes were identified following adipogenic differentiation.

To examine the cell migration potential ex vivo (Figure 4A), a sample of diseased meniscus tissue was placed on the scraped side of a tissue culture flask that had been 80% confluent with GFP-labeled primary meniscus cells. After 3 days, green cells were found inside the tissue sample (Figure 4B), which was confirmed by placing the sample in a new flask (Figure 4C). After an additional 7–10 days, cells, both green and unlabeled, residing in the damaged meniscus sample, were again found outside the tissue. Strikingly, cells migrated only into diseased meniscus tissues and not into the ones containing an intact superficial zone. Furthermore, a standard Boyden chamber assay revealed that the meniscus-derived cells displayed enhanced migration toward a gradient of human recombinant



platelet-derived growth factor (PDGF) (Figure 4D), much like the behavior recorded for chondrogenic progenitor cells (Koelling et al., 2009). Taken together, the multilineage differentiation potential and the migration results enabled us to name the cells “meniscus progenitor cells” (MPCs).

### The Influence of TGF- $\beta$ 3, RUNX2, and SMADs on the Chondrogenic Potential of MPCs

Using real-time RT-PCR, we observed significantly higher levels of mRNA for *TGF- $\beta$ 3* (Figure 5A), *SMAD2* (Figure 5B), and *SMAD3* (Figure 5C) in the cells derived from healthier menisci, whereas *SOX9* was generally unchanged (Figure 5D). When examined by IHC, *SMAD1* perinuclear staining (Figure 5E), *SMAD2/3* (Figure 5F), and *SMAD4* (Figure 5G) were all detected in cells from diseased menisci. To further elucidate the possible connection of the disease stage with the TGF- $\beta$ /BMP pathways, we performed a human TGF- $\beta$ /BMP signaling pathway array and found significantly higher levels of mRNA for *SMAD7* (Figure 5H), *noggin* (Figure 5I), and *follistatin* (Figure 5J) in meniscus cells from diseased tissues.

Because TGF- $\beta$  enhances chondrogenesis of OA chondrocytes (van der Kraan et al., 2012), we treated MPCs with 10 ng/ml TGF- $\beta$ 3 (Figure 6A). MPCs exposed to TGF- $\beta$ 3 exhibited significantly greater levels of *SMAD2/3* (Figure 6B) and also significantly greater levels of p-*SMAD2* (Figure 6C). Treatment with TGF- $\beta$ 3 also increased the levels of *SOX9* in the MPCs compared with controls (Figure 6D) while also decreasing *RUNX2* levels significantly (Figure 6E). In contrast, MPCs treated with 10 ng/ml BMP2 (an activator of the *SMAD1/5/7* axis) showed significantly reduced mRNA levels of *SMAD2* (Figure 6F) and *SOX9* (Figure 6G). When *RUNX2* was knocked down in MPCs by small interfering RNA (siRNA) interference (Figures 7A and 7B), *SMAD2/3* levels increased (Figure 7C); more importantly, p-*SMAD2* became detectable only after the *RUNX2* knock-down (Figure 7D).

Moreover, although the overexpression of *SMAD1* or *SMAD2* in MPCs (Figures 7E–7G) significantly increased *SOX9* expression (Figure 7H), *SMAD2* overexpression was more effective in reducing *RUNX2* levels than *SMAD1* overexpression (Figure 7I). These results demonstrate that the chondrogenic potential of MPCs is likely to be controlled by TGF- $\beta$ 3-mediated phosphorylation of *SMAD2*, which, in turn, upregulates *SOX9* and downregulates *RUNX2*.

## DISCUSSION

By employing a simple histopathological grading system, we have been able to separate OA tissue from patients

undergoing knee replacement into samples of early OA (healthier specimens) and severe degenerative disease (diseased specimens). The discriminative power of our grading system was validated by transcriptome analysis, where the molecular pattern found in diseased samples was distinct from that found in early stage OA meniscus. Differential expression patterns have also been shown before in menisci of different age (Rai et al., 2013). Previous results (Koelling et al., 2009; Seol et al., 2012) indicated the existence of progenitor cells in cartilage tissues from late stage OA, and, in fact, when we performed explant cultures using diseased meniscus tissue, we found cells migrating out of these specimens after a few days, which was not observed for healthier menisci. The intact superficial zone, with its flattened cells positive for collagen type I (Chevrier et al., 2009; Hellio Le Graverand et al., 2001) appear to be a barrier for cell migration. When removed, cells are able to migrate out of the less diseased samples. However, cell migration is more effective in diseased meniscus, indicating that inflammation and matrix degrading mediators are needed for migration. FACS analysis of these migratory meniscal cells showed that they were positive for well-known stem cell markers including *STRO-1*, *CD105*, or *CD106*. We also determined that these highly migratory meniscal-derived cells were multipotent; they synthesized collagen type II and suppressed *RUNX2* in 3D culture when grown in chondrogenic medium and they can be differentiated into the osteoblastic and adipogenic lineage. Interestingly, a significant difference in marker expression was observed when we compared cells migrating out of diseased meniscal explants with cells derived from meniscal tissue digestions, which indicates that the migratory progenitor cells are a subpopulation of the cells found in diseased human meniscus tissue in vivo. When the protein expression characteristics of the MSC markers are considered together with their clonicity, multipotency, and migratory potential, we named these cells meniscus progenitor cells (MPCs). The cells show signs of senescence (data not shown); therefore, we prefer the term progenitor rather than stem cell.

MPCs are decidedly different from the recently described CPCs (Koelling et al., 2009; Koelling and Miosge, 2010) not only due to their tissue origin and stem cell marker pattern, but also due to their ability to produce collagen type I and type II. However, they are similar as they also appear to be modulated via a balance between *RUNX2* and *SOX9* (Muhammad et al., 2013). Despite the presence of these multipotent cells in diseased human meniscus, they are not able to contribute substantially to regeneration efforts. Although the cell clusters found might be interpreted as signs of proliferation of the progenitor cells, it is likely that the numerous mediators of inflammation and tissue degeneration present, especially, in the late stages of OA

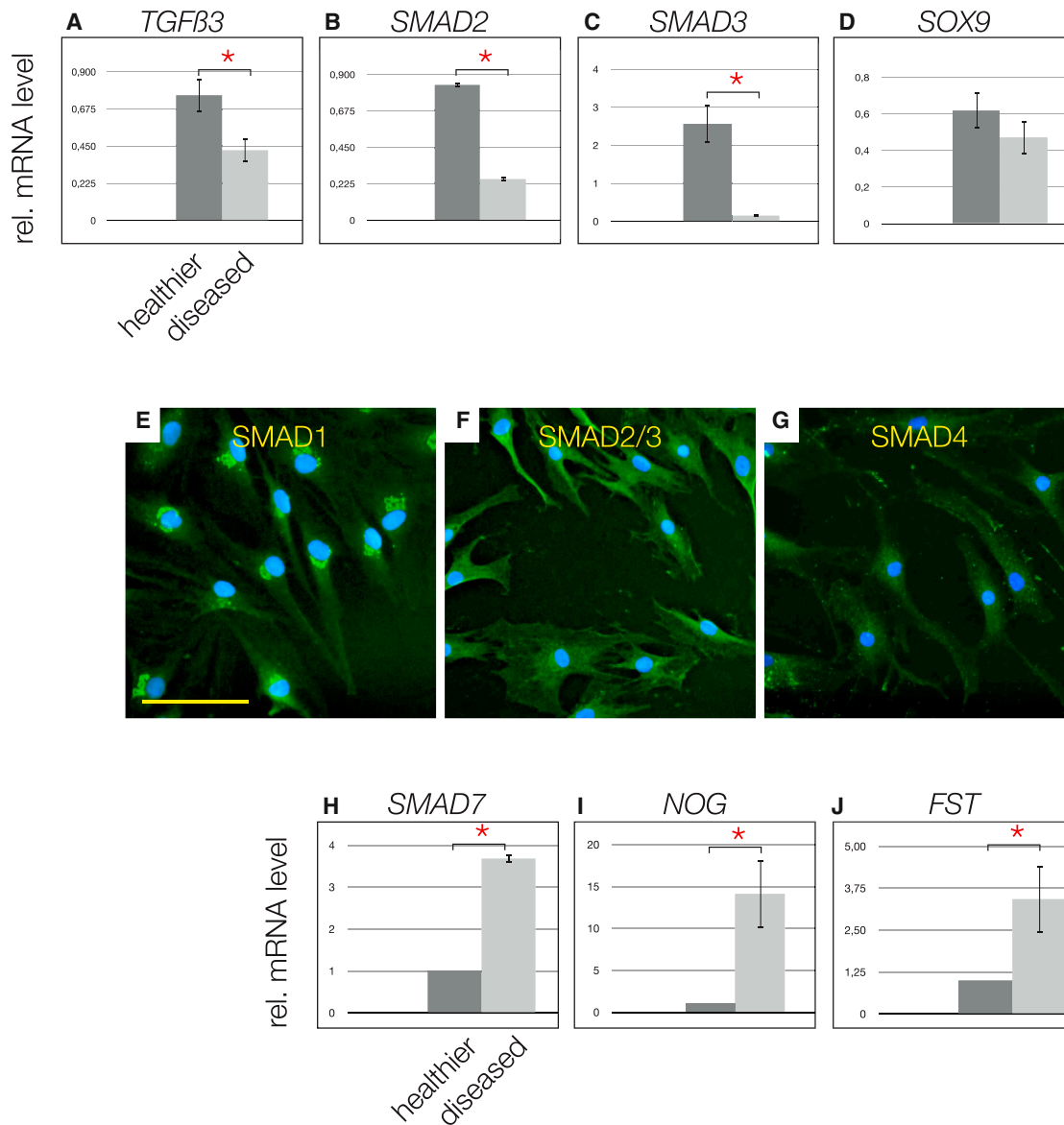


**Figure 5. TGF- $\beta$  Pathway Players in MPCs**

(A–C) *TGF- $\beta$ 3* mRNA levels are significantly higher in cells from healthier samples (A), which is consistent with *SMAD2* (B) and *SMAD3* (C) mRNA.

(D) No significant difference was observed for *SOX9* mRNA; however, a tendency toward higher levels in cells derived from healthier tissue was noted.

(E–G) Immunocytochemistry of inner diseased meniscal cells positive for *SMAD1* (E); note the punctuate perinuclear pattern, *SMAD2/3* (F), and *SMAD4* (G).

(H–J) The human PCR array for the TGF- $\beta$ /BMP pathway revealed high levels of mRNA of inhibitors of the TGF- $\beta$ /BMP axis, for example, *SMAD7* (H) noggin (I), follistatin (J), in cells obtained from inner diseased meniscus.

\*Significant differences ( $p \leq 0.05$ ); error bars denote the means  $\pm$  SD of three different healthier and three different diseased samples of OA patients. Scale bar, 150  $\mu$ m in (E)–(G).

investigated here, inhibit the regenerative capacity of any stem cell present in the diseased tissue.

In articular cartilage, deletion of the type 2 TGF- $\beta$  receptor results in the upregulation of RUNX2, MMP13, and

ADAMT55, which correlates with the progression of OA disease (Shen et al., 2013), and stimulation of SMAD2/3 signaling in articular chondrocytes has been suggested as a potential therapeutic manipulation for the treatment of

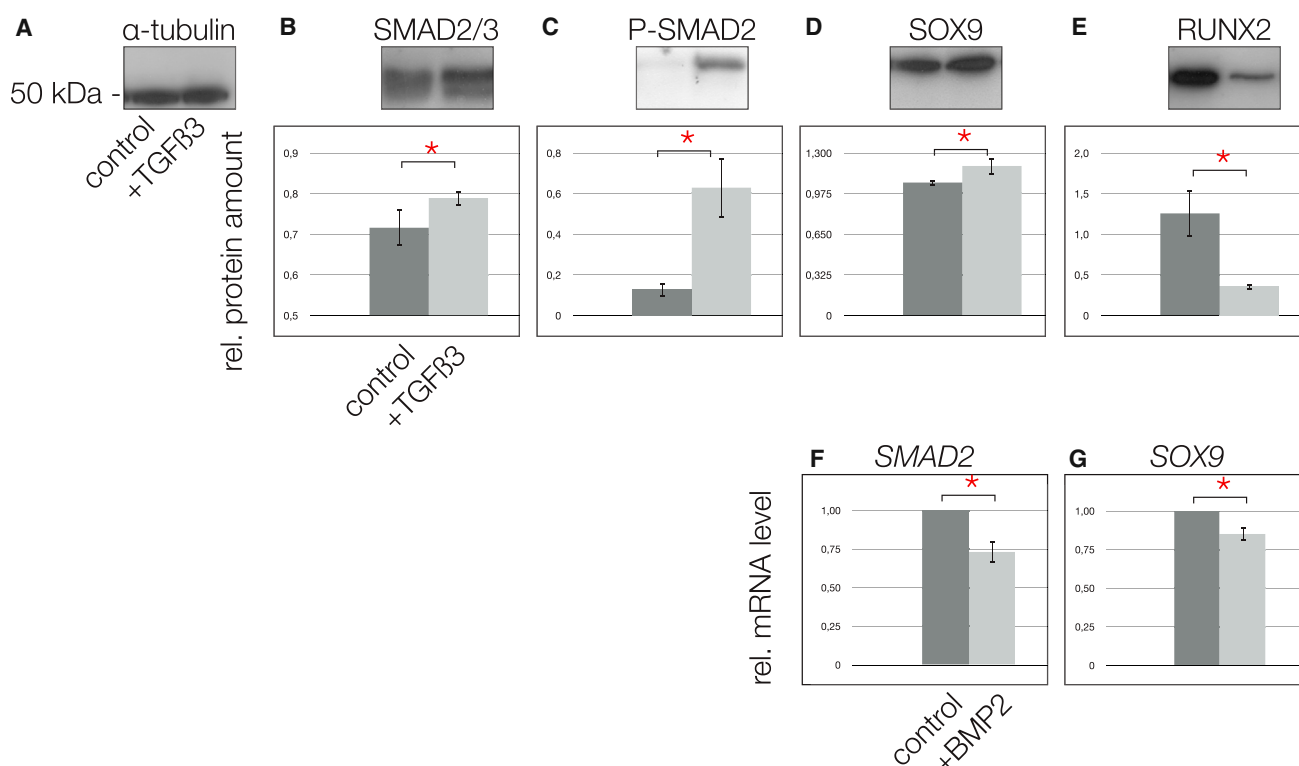


**Figure 6. The Effect of TGF-β on MPCs**

(A)  $\alpha$ -Tubulin indicates equal loading of the gel lanes; also in this figure, the first lanes in the blots and the dark gray bars in the graphs represent control experiments, whereas the second lanes and the light gray bars represent the TGF- $\beta$  stimulation experiments.

(B and C) Following stimulation of MPCs with 10 ng/ml TGF- $\beta$  for 24 hr, total SMAD2/3 (B) was significantly increased and active p-SMAD2 was significantly upregulated (C).

(D and E) In turn, SOX9 increased significantly (D) and RUNX2 was reduced significantly (E).

(F and G) In contrast, following stimulation of MPCs with 10 ng/ml BMP2 for 24 hr, total SMAD2 was reduced significantly (F), as well as SOX9 (G), shown by real-time RT-PCR.

\*Significant differences ( $p \leq 0.05$ ); error bars denote the means  $\pm$  SD of three individual experiments.

OA (van der Kraan et al., 2012). Here, we demonstrate that the treatment of MPCs with TGF- $\beta$  results in an upregulation of SOX9 and a downregulation of RUNX2 similar to findings in articular cartilage. The shift in articular chondrocytes from SMADS2/3 to SMADS1/5 appears to be important for the development of OA, and, recently, a balancing role of endoglin (CD 105) for this shift has been highlighted (Finnson et al., 2010). This change in pathway mediators may also be the case in the diseased human meniscus, because we found lower levels of SMAD2/3 and higher levels of RUNX2 in diseased tissue compared with healthier meniscus tissue.

The complex regulatory role of the signaling balance between TGF- $\beta$ /BMP in OA pathology is widely acknowledged (Finnson et al., 2010; van der Kraan et al., 2010), and our data suggest this interaction also governs meniscal cell behavior. We observe that MPCs from less diseased meniscus respond to TGF- $\beta$  via the ALK5 receptor, and

that this promotes chondrogenesis, whereas MPCs from more diseased meniscus are prone toward osteogenesis. Furthermore, our findings suggest that specific components of the TGF- $\beta$  pathway may be suitable targets for regenerative therapies directed at diseased human meniscus in late stages of OA. As OA is a very complex disease, and multiple tissues that are integral to joint function are impacted in different ways (Loeser et al., 2012), we find it unlikely that direct TGF- $\beta$  treatment of the meniscus will have significant therapeutic benefit, and undesirable side effects of TGF- $\beta$  therapy have been reported, including synovial hyperplasia, inflammation, or even osteophyte formation (Blaney Davidson et al., 2006; van Beuningen et al., 1998). Our current finding supports the notion that a more nuanced understanding of the regulatory events governing MPCs biology will be necessary to identify a cell-based therapy and the modulatory factors that support using these cells for meniscal regeneration. Identification



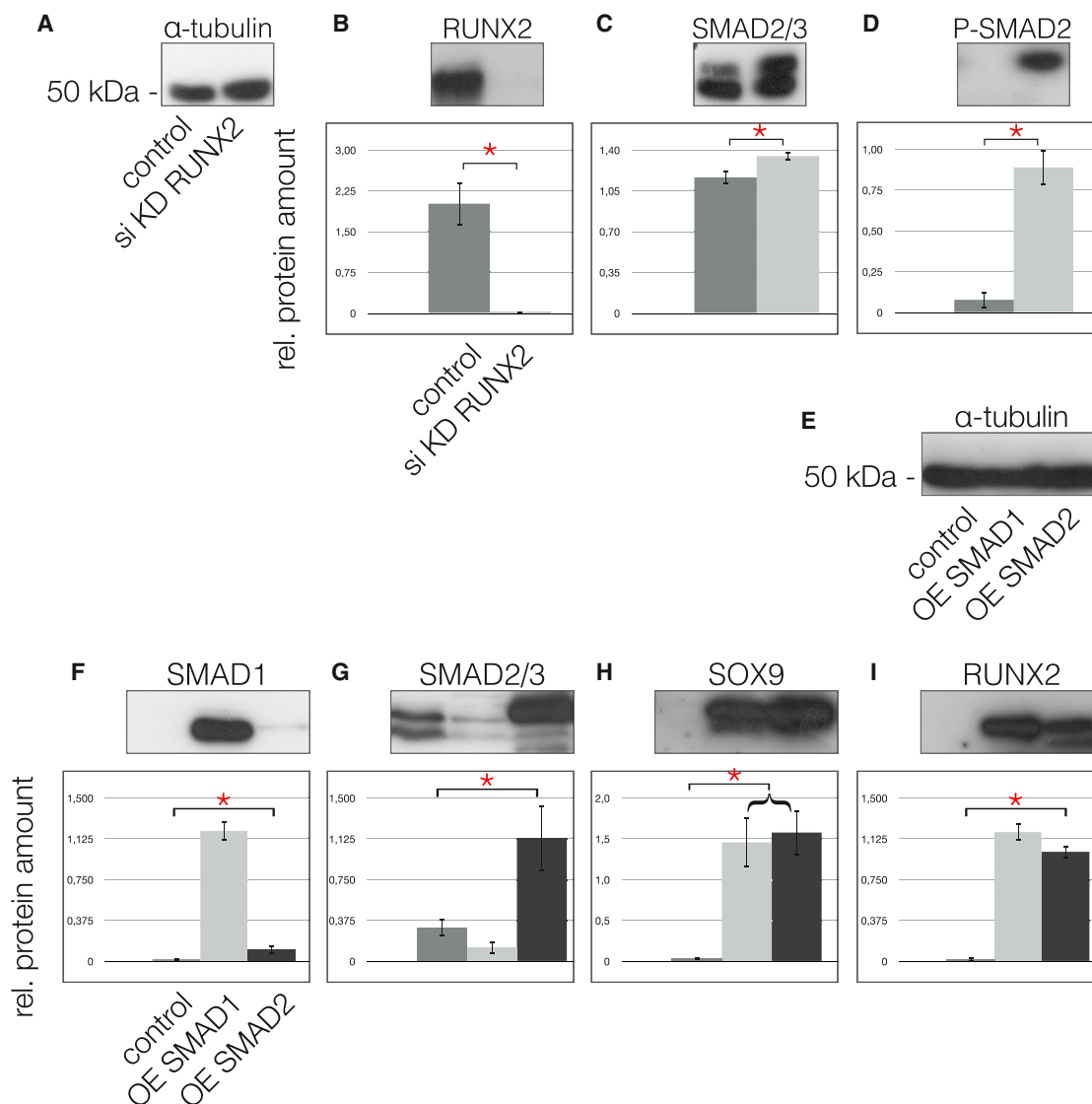


**Figure 7. Knockdown of RUNX2 and Overexpression of SMADs**

(A) α-tubulin was used for the quantification with ImageJ64; the first lanes of the blots always represent the controls as do the gray bars in the graphs, whereas the second lanes of the blots and the light gray bars of the graphs always represent the RUNX2 KD.

(B) Following RUNX2 KD, the protein was undetectable (lane 2) compared with the control (lane 1).

(C–E) In turn, total SMAD2/3 increased significantly (C) and enabled the detection of p-SMAD2 (D). Overexpression (OE) of SMAD1 and SMAD2. (E) α-tubulin was applied for quantification, the first lanes of the blots always represent the controls as do the dark gray bars in the graphs. The second lanes and the light gray bars represent SMAD1 OE. Finally, the third lanes of the blots and the black bars of the graphs represent the OE of SMAD2.

(F) SMAD1 OE is seen in lane 2.

(G) SMAD2 OE is seen in lane 3.

(H) OE of SMAD1 and SMAD2 results in a significant upregulation of SOX9.

(I) OE of SMAD2 results in a greater reduction of RUNX2 as does OE of SMAD1.

\*Significant differences ( $p \leq 0.05$ ); error bars denote the means  $\pm$  SD of three individual experiments.

and characterization of MPCs provides direct evidence that meniscal repair cells are present in highly diseased tissue and also allows for detailed study of the signaling pathways

that govern their proliferation and differentiation, a first step in identifying drug targets for the regeneration of diseased meniscus.



## EXPERIMENTAL PROCEDURES

### Tissues and Preparation

Adult osteoarthritic lateral and medial menisci were obtained from more than 150 patients (ages 62–75 years) suffering from late-stage OA after total knee replacement operations. The patients met the American College of Rheumatology classification criteria and provided their written informed consent. Histopathological classification of OA cartilage confirmed the presence of late-stage OA (Pritzker et al., 2006) of the tibial plateau and femoral condyles in all samples.

### Histology and Meniscus Grading

For light microscopy, meniscus specimens ( $n = 80$ ), including the white and red areas (Figure 1A, inset), were processed as described previously (Koelling and Miosge, 2010), and a combined Alcian blue/nuclear fast-red staining was performed. Based on existing grading systems (Pauli et al., 2011; Zhang et al., 2011), we developed a simple score for meniscus degradation. The presence (1 point) or absence (2 points) of the superficial zone and the intensity of the Alcian blue staining (high = 1 point or low = 2 points) were used for evaluations. The presence of fatty degeneration and/or cell clusters (2 points) or the presence of calcifications (3 points) was also included. A minimum of 2 and a maximum score of 9 points can be reached. The threshold was set to 4 points. Three independent histologists evaluated more than 40 samples and identified 31 with a score of above 4 (diseased) and 16 with scores of below 4 (healthier). The remaining samples were not evaluated unequivocally.

### Cell Isolation and Culture

Tissue pieces measuring 7–10 mm<sup>3</sup> from the central inner zone (white area) of the healthier ( $n = 12$ ) and diseased ( $n = 12$ ) human menisci were excised, and care was taken not to include the outer red zone. Samples of healthier menisci with an intact superficial zone (grading score: 2,  $n = 12$ ) were also excised. After 7–10 days of incubation, only samples that lacked a superficial zone showed outgrowth of cells, which were harvested, and 10<sup>3</sup> cells/cm<sup>2</sup> were transferred to a monolayer culture under standard conditions. 3D culturing was performed using alginate beads. Samples of 2–3 mm<sup>3</sup> in size from the superficial area of healthier menisci ( $n = 7$ ) and the central area of diseased menisci ( $n = 7$ ) were harvested and digested with collagenase I (152 U/ml; Invitrogen), collagenase II (280 U/ml; Biochrom), and dispase (15 U/ml; Invitrogen) for 6 hr at 37°C.

### Microarray Analysis and Bioinformatic Methods

Quality control and the quantification of total RNA samples was performed, and data from ten human samples were measured using the microarray (Microarrays) ReadyArray (HS1100), which contains 48,958 probes per microarray slide from the Stanford/Illumina collaboration on the HEEBO (Human Exonic Evidence Based Oligonucleotide) set of long oligos. This chip was used in a one-color assay with a reference measurement of internal house-keeping genes. An internal QC was run and data were curated, primarily from nonzero flag values that indicate absent or poor-quality spots, resulting in 13,585 probes. Next, quantile-normali-

zation and logarithmizing followed. We then arbitrarily selected 15 potential marker genes, TIMP1, TIMP2, TIMP3, COL3A1, RUNX2, SOX9, ACAN, PRG4, DCN, MMP9, MMP3, MMP14, ADAMTS20, ADAMTS1, and NID2 (all known to be involved in the pathogenesis of OA), to determine whether each of the ten samples belonged to the “diseased” or “healthier” group. A Pearson correlation-based hierarchical clustering approach including row scaling and Ward’s minimum variance method was chosen. This analysis revealed two groups of four samples each. For the selected eight samples, a differential expression analysis including all 13,585 probes with an empirical Bayes statistic of the limma package, moderated gene-by-gene *t* tests and *p* value adjustments via the Benjamini-Hochberg method was performed.

### Proteome Analysis

In-gel digestion and peptide extraction was performed using aqueous acetonitrile, and mass spectrometric analysis was performed as described (Christian et al., 2014). The eluent was analyzed using a Top10 method in the Data Dependent Acquisition mode on the Q Exactive high-resolution mass spectrometry system (Thermo Scientific) operated under Tune 2.2 using HCD fragmentation, with normalized collision energy of 25%. Peak lists were generated using the Raw2MSM v1.10 software (MPI for Biochemistry, Martinsried, Germany). All MS/MS samples were analyzed using Mascot (Matrix Science, v.2.4.1) set to search the NCBI nr\_20130805 database (selected for *Homo sapiens*, 251,430 entries). Further details, especially about normalization procedures, have already been published (Christian et al., 2014).

### Antibodies

Monoclonal anti-type II collagen (CIIC1, 1:500) and anti-STRO1 (STRO1, 1:100) antibodies were obtained from the Developmental Studies Hybridoma Bank, University of Iowa. For western blotting, monoclonal  $\alpha$ -tubulin (T6199, 1:2,000, Sigma-Aldrich), anti-SMAD2/3 (c-8, sc-133098, 1:1,000), anti-SMAD1 (A-4, sc-7965, 1:1,000), anti-SOX9 (H-90, sc-2095, 1:1,000), anti-RUNX2 (M-70, sc10758, 1:1,000), anti-SMAD4 (B-8, sc-7966, 1:1,000), anti-TGF- $\beta$ 3 (III, sc-83, 1:100), anti-collagen type I (C-18, sc-8784, 1:100), and anti-ALK1 (c20, sc-19547, 1:100) antibodies were from SC Biotechnology. Polyclonal anti-phospho-SMAD2 (Ser465/467, #3101, 1:1,000) purchased from Cell Signaling Technology, and anti-ALK5 antibodies (Ab-165, E11-1126B, 1:100) from EnoGene Biotech. FACS analysis was performed with PE-coupled anti-CD29 (#554543, 1:500), CD34 (#345802, 1:200), CD106 (#551146, 1:500), and fluorescein isothiocyanate (FITC)-coupled anti-CD45 (#345808, 1:200), CD105 (#312404, 1:500) antibodies from BD Pharmingen. Anti-CD90-PE (#328110, 1:200) was from BioLegend. All secondary antibodies were the ones used previously (Koelling et al., 2009).

### Immunohistochemistry

Ten diseased and ten healthier samples were processed for immunohistochemistry with the HiDefDetection alkaline phosphatase mouse/rabbit system (Cell Marque). Immunoreactions were also performed with swine serum as a negative control, and figures show representatives of three different healthier and three different more diseased samples of OA patients.



### Immunoblotting

Immunoblotting was performed as described previously (Koelling et al., 2009) and quantified using  $\alpha$ -tubulin as a loading control using the ImageJ64 program.

### RNA extraction and cDNA Synthesis

Cells from samples of healthier and diseased menisci in P1 monolayer cultures were lysed directly in RLT buffer and subjected to RNA isolation (RNeasy Mini Kit, QIAGEN) as described (Koelling et al., 2009).

### Quantitative Real-Time RT-PCR

A 10  $\mu$ l volume per PCR comprising 1 ng of cDNA, 5  $\mu$ l of Platinum Sybr Green qPCR SuperMix (Invitrogen) and 20 pmol of each primer was chosen. The program primer 3 (<http://bioinfo.ut.ee/primer3-0.4.0/>) was used to design the primers (Table 1).

PCRs were performed as described previously, and data were normalized to a highly consistent housekeeping gene ( $\beta$ 2M). PCR products were sequenced (SeqLab), and relative ratios were calculated (Pfaffl, 2001). Every PCR was run three times in triplicate. The intratest and intertest variations were <1%. Primer efficiencies ranged from 1.9 to 2.1.

### Cell Differentiation

Chondrogenic differentiation was performed using 3D cell culture as described previously (Koelling et al., 2009). For osteogenic differentiation, a total of 1,000 MPCs/cm<sup>2</sup> in 75 cm<sup>2</sup> flasks were differentiated into cells of the osteoblastic lineage under the influence of NH OsteoDiffMedium or adipogenic differentiation was performed using NH AdipoDiffMedium (Miltenyi Biotec).

### Immunofluorescence Microscopy

P1 cells were grown on coverslips, fixed, and incubated with 100  $\mu$ l of primary antibody (1:50 dilution in PBS) for 1 hr at room temperature. In the case of uncoupled primary antibodies, we then added secondary fluorescence-coupled antibodies (1:500 dilution in PBS) for 20 min at room temperature and stained with DAPI.

### FACS Analysis

To test cells for stem cell markers, 10<sup>6</sup> cells were suspended in 100  $\mu$ l of PBS containing 1  $\mu$ l of fluorescence-coupled antibody at room temperature for 1 hr in the dark. Anti-human-PE/FITC immunoglobulin isotype antibodies (BD Pharmingen) served as negative controls for gating. The cells were then washed twice, centrifuged, and subjected to FACS analysis using a FACScan machine (Becton Dickinson), and 10,000 living cells were analyzed (Koelling et al., 2009). For data evaluation, we used the WinMDiv2.9 program (Scripps Research Institute). The FACS Vantage SE (Becton Dickinson) was applied for cell selection and the Cell Quest Pro 2000 software package was used for analysis.

### PCR Array

The human TGF- $\beta$ /BMP signaling pathway array was used (PAHS-035ZA\_0123, SABiosciences), according to the manufacturer's instructions, and data were normalized using the standard program of the company's online platform.

### GFP Transfection

The cells ( $5 \times 10^5$ ) were transfected with 2.5  $\mu$ g of the pmaxGFP vector (Lonza, Koeln, Germany) in 100  $\mu$ l of nucleofector solution using the Amaxa program U-23 as described before (Koelling et al., 2009).

### Migration and Integration Assay

In an ex vivo assay, a sample of diseased meniscus tissue was placed on the scraped side of a flask that had been 80% confluent with GFP-labeled cells. After 5–7 days, the specimens were washed with PBS, transferred to a new flask and examined using a fluorescence microscope. For the in vitro migration assay, we used a commercial two-chamber system (CytoSelect, Cell Biolabs) and extinctions were measured at 560 nm. Human recombinant PDGF (R&D Systems, 10 ng/ml) was applied as chemoattractant.

### Cell Induction Experiment

Cells in 3D alginate were stimulated using recombinant human BMP2 (10 ng/ml, lot# MSA3612112) and TGF- $\beta$ 3 (10 ng/ml, lot# MSA3612112), both of which were obtained from R&D Systems. After 24 hr, the cells were harvested and subjected to total protein and RNA extraction.

### siRNA Transfections

The iLenti-GFP siRNA expression vector (ABM) was used for RUNX2 knockdown. The probe (CAGCACGCTATTAAATCCA AATT) that targeted Runx2 was placed under the control of H1/H6 and the GFP sequence under the CMV promoter. Control experiments were performed using a vector containing a scrambled siRNA sequence or without any vector. For the transfection of cells, see above.

### Overexpression

SMAD1 and SMAD2 cloned into the pCMV5-Flag and pCMV5B-HA vectors were purchased from Addgene, Cambridge, USA and sequenced to verify the inserts. The cells were transfected either with the expression vector or the vector without the insert, as described above.

### Statistical Analyses

Statistical product and service solutions (SPSS) software version 13.0 was used. The observed data were tested statistically, and the representative data shown are the means and standard deviation of at least three different healthier and three different more diseased samples of OA patients, if not stated otherwise. After testing for normality of distribution and homogeneity of variances, we performed ANOVAs and post hoc pairwise comparisons of the mean values. The Pearson correlation coefficients were calculated to examine the relationships between parameters. A p value < 0.05 was considered significant.

### ACCESSION NUMBERS

Data were submitted to Gene Expression Omnibus under accession number GSE52042.





## AUTHOR CONTRIBUTIONS

Contributions were as follows: H.M., study conception, study design, acquisition of data, analyses and interpretation of data, manuscript preparation, and statistical analyses; B.S., study conception, study design, acquisition of data, analyses and interpretation of data, manuscript and figure preparation, and statistical analyses; C.B., acquisition of data; M.R., acquisition of data; J.A., acquisition of data; S.v.d.H., microarray analysis and bioinformatic methods; V.R., study conception, study design, interpretation of data, and manuscript preparation; and N.M., study conception, study design, interpretation of data, and manuscript preparation.

## ACKNOWLEDGMENTS

The authors would like to thank Professor H. Urlaub and Dr. C. Lenz from the joint proteome facility at the MPI for Biophysical Chemistry, Goettingen and the Medical Faculty of the University of Goettingen. We would also like to thank Dr. K. Jung from the Institute of Medical Statistics, Medical Faculty Goettingen.

Received: April 2, 2014

Revised: August 19, 2014

Accepted: August 20, 2014

Published: September 25, 2014

## REFERENCES

- Benjamin, M., and Evans, E.J. (1990). Fibrocartilage. *J. Anat.* **171**, 1–15.
- Blaney Davidson, E.N., Vitters, E.L., van der Kraan, P.M., and van den Berg, W.B. (2006). Expression of transforming growth factor-beta (TGFbeta) and the TGFbeta signalling molecule SMAD-2P in spontaneous and instability-induced osteoarthritis: role in cartilage degradation, chondrogenesis and osteophyte formation. *Ann. Rheum. Dis.* **65**, 1414–1421.
- Brophy, R.H., Rai, M.F., Zhang, Z., Torgomyan, A., and Sandell, L.J. (2012). Molecular analysis of age and sex-related gene expression in meniscal tears with and without a concomitant anterior cruciate ligament tear. *J. Bone Joint Surg. Am.* **94**, 385–393.
- Chevrier, A., Nelea, M., Hurtig, M.B., Hoemann, C.D., and Buschmann, M.D. (2009). Meniscus structure in human, sheep, and rabbit for animal models of meniscus repair. *J. Orthop. Res.* **27**, 1197–1203.
- Christian, H., Hofele, R.V., Urlaub, H., and Ficner, R. (2014). Insights into the activation of the helicase Prp43 by biochemical studies and structural mass spectrometry. *Nucleic Acids Res.* **42**, 1162–1179.
- de Mulder, E.L., Hannink, G., Giele, M., Verdonchot, N., and Buma, P. (2013). Proliferation of meniscal fibrochondrocytes cultured on a new polyurethane scaffold is stimulated by TGF- $\beta$ . *J. Biomater. Appl.* **27**, 617–626.
- Englund, M., Guermazi, A., Gale, D., Hunter, D.J., Aliabadi, P., Clancy, M., and Felson, D.T. (2008). Incidental meniscal findings on knee MRI in middle-aged and elderly persons. *N. Engl. J. Med.* **359**, 1108–1115.
- Englund, M., Roemer, F.W., Hayashi, D., Crema, M.D., and Guermazi, A. (2012). Meniscus pathology, osteoarthritis and the treatment controversy. *Nat Rev Rheumatol* **8**, 412–419.
- Finnson, K.W., Parker, W.L., Chi, Y., Hoemann, C.D., Goldring, M.B., Antoniou, J., and Philip, A. (2010). Endoglin differentially regulates TGF-beta-induced Smad2/3 and Smad1/5 signalling and its expression correlates with extracellular matrix production and cellular differentiation state in human chondrocytes. *Osteoarthritis Cartilage* **18**, 1518–1527.
- Goumans, M.J., Valdimarsdottir, G., Itoh, S., Lebrin, F., Larsson, J., Mummery, C., Karlsson, S., and ten Dijke, P. (2003). Activin receptor-like kinase (ALK)1 is an antagonistic mediator of lateral TGFbeta/ALK5 signaling. *Mol. Cell* **12**, 817–828.
- Haddad, B., Pakravan, A.H., Konan, S., Adesida, A., and Khan, W. (2013). A systematic review of tissue engineered meniscus: cell-based preclinical models. *Curr. Stem Cell Res. Ther.* **8**, 222–231.
- Haider, S., and Pal, R. (2013). Integrated analysis of transcriptomic and proteomic data. *Curr. Genomics* **14**, 91–110.
- Hellio Le Graverand, M.P., Vignon, E., Otterness, I.G., and Hart, D.A. (2001). Early changes in lapine menisci during osteoarthritis development: part I: cellular and matrix alterations. *Osteoarthritis Cartilage* **9**, 56–64.
- Hommen, J.P., Applegate, G.R., and Del Pizzo, W. (2007). Meniscus allograft transplantation: ten-year results of cryopreserved allografts. *Arthroscopy* **23**, 388–393.
- Koelling, S., and Miosge, N. (2010). Sex differences of chondrogenic progenitor cells in late stages of osteoarthritis. *Arthritis Rheum.* **62**, 1077–1087.
- Koelling, S., Kruegel, J., Irmer, M., Path, J.R., Sadowski, B., Miro, X., and Miosge, N. (2009). Migratory chondrogenic progenitor cells from repair tissue during the later stages of human osteoarthritis. *Cell Stem Cell* **4**, 324–335.
- Loeser, R.F. (2013). Aging processes and the development of osteoarthritis. *Curr. Opin. Rheumatol.* **25**, 108–113.
- Loeser, R.F., Goldring, S.R., Scanzello, C.R., and Goldring, M.B. (2012). Osteoarthritis: a disease of the joint as an organ. *Arthritis Rheum.* **64**, 1697–1707.
- Lohmander, L.S., and Roos, E.M. (2007). Clinical update: treating osteoarthritis. *Lancet* **370**, 2082–2084.
- Lohmander, L.S., Englund, P.M., Dahl, L.L., and Roos, E.M. (2007). The long-term consequence of anterior cruciate ligament and meniscus injuries: osteoarthritis. *Am. J. Sports Med.* **35**, 1756–1769.
- Massagué, J. (2012). TGF $\beta$  signalling in context. *Nat. Rev. Mol. Cell Biol.* **13**, 616–630.
- Mauck, R.L., Martinez-Diaz, G.J., Yuan, X., and Tuan, R.S. (2007). Regional multilineage differentiation potential of meniscal fibrochondrocytes: implications for meniscus repair. *Anat. Rec. (Hoboken)* **290**, 48–58.
- McDevitt, C.A., and Webber, R.J. (1990). The ultrastructure and biochemistry of meniscal cartilage. *Clin. Orthop. Relat. Res.* (252), 8–18.



- Muhammad, H., Schminke, B., and Miosge, N. (2013). Current concepts in stem cell therapy for articular cartilage repair. *Expert Opin. Biol. Ther.* **13**, 541–548.
- Osawa, A., Harner, C.D., Gharaibeh, B., Matsumoto, T., Mifune, Y., Kopf, S., Ingham, S.J., Schreiber, V., Usas, A., and Huard, J. (2013). The use of blood vessel-derived stem cells for meniscal regeneration and repair. *Med. Sci. Sports Exerc.* **45**, 813–823.
- Pauli, C., Grogan, S.P., Patil, S., Otsuki, S., Hasegawa, A., Koziol, J., Lotz, M.K., and D'Lima, D.D. (2011). Macroscopic and histopathologic analysis of human knee menisci in aging and osteoarthritis. *Osteoarthritis Cartilage* **19**, 1132–1141.
- Petersen, W., Pufe, T., Stärke, C., Fuchs, T., Kopf, S., Raschke, M., Becker, R., and Tillmann, B. (2005). Locally applied angiogenic factors—a new therapeutic tool for meniscal repair. *Ann. Anat.* **187**, 509–519.
- Pfaffl, M.W. (2001). A new mathematical model for relative quantification in real-time RT-PCR. *Nucleic Acids Res.* **29**, e45.
- Poole, C.A., Ayad, S., and Gilbert, R.T. (1992). Chondrons from articular cartilage. V. Immunohistochemical evaluation of type VI collagen organisation in isolated chondrons by light, confocal and electron microscopy. *J. Cell Sci.* **103**, 1101–1110.
- Pritzker, K.P., Gay, S., Jimenez, S.A., Ostergaard, K., Pelletier, J.P., Revell, P.A., Salter, D., and van den Berg, W.B. (2006). Osteoarthritis cartilage histopathology: grading and staging. *Osteoarthritis Cartilage* **14**, 13–29.
- Rai, M.F., Patra, D., Sandell, L.J., and Brophy, R.H. (2013). Transcriptome analysis of injured human meniscus reveals a distinct phenotype of meniscus degeneration with aging. *Arthritis Rheum.* **65**, 2090–2101.
- Reginster, J.Y. (2002). The prevalence and burden of arthritis. *Rheumatology (Oxford)* **41** (Supp 1), 3–6.
- Segawa, Y., Muneta, T., Makino, H., Nimura, A., Mochizuki, T., Ju, Y.J., Ezura, Y., Umezawa, A., and Sekiya, I. (2009). Mesenchymal stem cells derived from synovium, meniscus, anterior cruciate ligament, and articular chondrocytes share similar gene expression profiles. *J. Orthop. Res.* **27**, 435–441.
- Seol, D., McCabe, D.J., Choe, H., Zheng, H., Yu, Y., Jang, K., Walter, M.W., Lehman, A.D., Ding, L., Buckwalter, J.A., and Martin, J.A. (2012). Chondrogenic progenitor cells respond to cartilage injury. *Arthritis Rheum.* **64**, 3626–3637.
- Shen, J., Li, J., Wang, B., Jin, H., Wang, M., Zhang, Y., Yang, Y., Im, H.J., O'Keefe, R., and Chen, D. (2013). Deletion of the transforming growth factor  $\beta$  receptor type II gene in articular chondrocytes leads to a progressive osteoarthritis-like phenotype in mice. *Arthritis Rheum.* **65**, 3107–3119.
- Steadman, J.R., and Rodkey, W.G. (2005). Tissue-engineered collagen meniscus implants: 5- to 6-year feasibility study results. *Arthroscopy* **21**, 515–525.
- Steinert, A.F., Palmer, G.D., Capito, R., Hofstaetter, J.G., Pilapil, C., Ghivizzani, S.C., Spector, M., and Evans, C.H. (2007). Genetically enhanced engineering of meniscus tissue using ex vivo delivery of transforming growth factor-beta 1 complementary deoxyribonucleic acid. *Tissue Eng.* **13**, 2227–2237.
- van Beuningen, H.M., Glansbeek, H.L., van der Kraan, P.M., and van den Berg, W.B. (1998). Differential effects of local application of BMP-2 or TGF-beta 1 on both articular cartilage composition and osteophyte formation. *Osteoarthritis Cartilage* **6**, 306–317.
- van der Kraan, P.M., Blaney Davidson, E.N., and van den Berg, W.B. (2010). Bone morphogenetic proteins and articular cartilage: to serve and protect or a wolf in sheep clothing's? *Osteoarthritis Cartilage* **18**, 735–741.
- van der Kraan, P.M., Goumans, M.J., Blaney Davidson, E., and ten Dijke, P. (2012). Age-dependent alteration of TGF- $\beta$  signalling in osteoarthritis. *Cell Tissue Res.* **347**, 257–265.
- Webber, R.J., York, J.L., Vanderschelden, J.L., and Hough, A.J., Jr. (1989). An organ culture model for assaying wound repair of the fibrocartilaginous knee joint meniscus. *Am. J. Sports Med.* **17**, 393–400.
- Woolf, A.D., and Pfleger, B. (2003). Burden of major musculoskeletal conditions. *Bull. World Health Organ.* **81**, 646–656.
- Zhang, D., Cheriyan, T., Martin, S.D., Gomoll, A.H., Schmid, T.M., and Spector, M. (2011). Lubricin distribution in the torn human anterior cruciate ligament and meniscus. *J. Orthop. Res.* **29**, 1916–1922.



# Biomechanical properties of murine meniscus surface via AFM-based nanoindentation

Qing Li<sup>a</sup>, Basak Doyran<sup>a</sup>, Laura W. Gamer<sup>b</sup>, X. Lucas Lu<sup>c</sup>, Ling Qin<sup>d</sup>, Christine Ortiz<sup>e</sup>, Alan J. Grodzinsky<sup>f,g,h</sup>, Vicki Rosen<sup>b</sup>, Lin Han<sup>a,\*</sup>

<sup>a</sup> School of Biomedical Engineering, Science, and Health Systems, Drexel University, Philadelphia, PA 19104, United States

<sup>b</sup> Department of Developmental Biology, Harvard School of Dental Medicine, Boston, MA 02115, United States

<sup>c</sup> Department of Mechanical Engineering, University of Delaware, Newark, DE 19716, United States

<sup>d</sup> Department of Orthopaedic Surgery, University of Pennsylvania, Philadelphia, PA 19104, United States

<sup>e</sup> Department of Materials Science and Engineering, Massachusetts Institute of Technology, Cambridge, MA 02139, United States

<sup>f</sup> Department of Biological Engineering, Massachusetts Institute of Technology, Cambridge, MA 02139, United States

<sup>g</sup> Department of Electrical Engineering and Computer Science, Massachusetts Institute of Technology, Cambridge, MA 02139, United States

<sup>h</sup> Department of Mechanical Engineering Massachusetts Institute of Technology, Cambridge, MA 02139, United States

## ARTICLE INFO

### Article history:

Accepted 28 February 2015

### Keywords:

Meniscus

Mouse models

Atomic force microscopy

Nanoindentation

Anisotropy

## ABSTRACT

This study aimed to quantify the biomechanical properties of murine meniscus surface. Atomic force microscopy (AFM)-based nanoindentation was performed on the central region, proximal side of menisci from 6- to 24-week old male C57BL/6 mice using microspherical tips ( $R_{tip} \approx 5 \mu\text{m}$ ) in PBS. A unique, linear correlation between indentation depth,  $D$ , and response force,  $F$ , was found on menisci from all age groups. This non-Hertzian behavior is likely due to the dominance of tensile resistance by the collagen fibril bundles on meniscus surface that are mostly aligned along the circumferential direction. The indentation resistance was calculated as both the effective modulus,  $E_{ind}$ , via the isotropic Hertz model, and the effective stiffness,  $S_{ind} = dF/dD$ . Values of  $S_{ind}$  and  $E_{ind}$  were found to depend on indentation rate, suggesting the existence of poro-viscoelasticity. These values do not significantly vary with anatomical sites, lateral versus medial compartments, or mouse age. In addition,  $E_{ind}$  of meniscus surface (e.g.,  $6.1 \pm 0.8 \text{ MPa}$  for 12 weeks of age, mean  $\pm$  SEM,  $n=13$ ) was found to be significantly higher than those of meniscus surfaces in other species, and of murine articular cartilage surface ( $1.4 \pm 0.1 \text{ MPa}$ ,  $n=6$ ). In summary, these results provided the first direct mechanical knowledge of murine knee meniscus tissues. We expect this understanding to serve as a mechanics-based benchmark for further probing the developmental biology and osteoarthritis symptoms of meniscus in various murine models.

© 2015 Elsevier Ltd. All rights reserved.

## 1. Introduction

Knee meniscus is a hydrated fibrocartilage tissue with an extracellular matrix (ECM) mainly composed of circumferentially aligned, type I-dominated collagen fibers ( $\approx 20$ – $25 \text{ wet wt\%}$ ) and small amounts of proteoglycans ( $< 5 \text{ wet wt\%}$ ) (Aspden et al., 1985; Herwig et al., 1984). In human menisci, the circumferential fibers are wrapped within the superficial layer made of radially aligned fibers, which is covered by a thin mesh of transversely aligned fibrils on the surface (Petersen and Tillmann, 1998). Within the interior of the meniscus, circumferential fibers are further interdigitated by “radial-tie” fibers throughout (Skaggs et al., 1994). This

hierarchically structured, heterogeneous ECM provides meniscus with its biomechanical functions paramount to joint motion, including load distribution (Walker and Erkman, 1975), shock absorption (Voloshin and Wosk, 1983) and lubrication (Fithian et al., 1990). During the progression of osteoarthritis (OA), meniscus often undergoes maceration, tear or even total damage that leads to the loss of its biomechanical functions (Katsuragawa et al., 2010). These symptoms contribute to the abnormal joint loading, and further accelerate the degeneration of cartilage (Englund, 2008; Hunter et al., 2006; Klompmaker et al., 1992). Knowledge about the structure-mechanics relationships of meniscus ECM is thus critical for understanding joint function, documenting disease progression and designing repair strategies (Makris et al., 2011).

In the past decades, the mechanical properties of menisci in human and animals have been extensively explored via both experimental (Baro et al., 2012; Fithian et al., 1990; Proctor et al., 1989;

\* Corresponding author. Tel.: +1 215 571 3821; fax: +1 215 895 4983.

E-mail address: [lh535@drexel.edu](mailto:lh535@drexel.edu) (L. Han).

Sweigart and Athanasiou, 2005) and theoretical (Spilker et al., 1992) approaches. These studies have established a knowledge base of meniscus biomechanics across species. However, biomechanical knowledge of meniscus in one critical species, mouse, is lacking. Murine models offer a unique platform to study synovial joint development and OA pathology due to its short lifespan, low cost of maintenance and availability for genetic modification (Ameje and Young, 2006; Fang and Beier, 2014). Limited by its relatively small tissue size, conventional mechanical tests are not applicable to evaluate the structure or mechanical properties of murine menisci. Without this understanding, it is challenging to study joint development or OA degradation in murine models from the perspective of meniscus biomechanics.

The objective of this study is to define the biomechanical properties of murine meniscus surface. Using atomic force microscopy (AFM)-based nanoindentation, we quantified the indentation responses of the meniscus surface from normal, male C57BL/6 mice. This study revealed the impacts of indentation rate, anatomical location and age on the mechanical properties. The indentation responses were interpreted in the context of meniscus surface collagen fibril structure quantified on 12-week old tissues. Results were compared with menisci from other species, as well as murine articular cartilage to highlight the unique properties of murine meniscus. We expect the knowledge learned from the evaluation of healthy murine meniscus to serve as a benchmark for future investigations of OA-associated mechanical symptoms of meniscus surface in various transgenic or surgery-induced murine models.

## 2. Methods

### 2.1. Sample preparation

Hind knee menisci were harvested from male C57BL/6 mice at 6, 8, 12 and 24 weeks of ages (The Jackson Laboratory, Bar Harbor, ME) via release from the meniscus-tibial tendons. Freshly dissected samples were maintained in phosphate buffered saline (PBS, pH=7.4) with protease inhibitors (Pierce Protease Inhibitor Tablets 88266, Thermo Fisher Scientific, Rockford, IL) at 4 °C for less than 24 h prior to mechanical tests. For each mouse, we tested the proximal side of both lateral and medial menisci. For the same mouse, we did not observe statistical differences in the mechanical properties of tissues from left versus right legs. We therefore tested either left or right knee menisci from one mouse, or pooled the data on the menisci of the same mouse.

Histology images were taken to show the overall morphology and location of ossification. Right knee joints from each of the 8- and 24-week old mice were harvested, decalcified, and embedded in paraffin. Serial 5- $\mu$ m-thick sagittal sections were cut across the joint medial compartment. Safranin-O/FastGreen staining images showed that ossification at the anterior and posterior horns increased with age, with larger ossicles at the anterior end (Fig. 1a). This observation was consistent with previous studies (Pedersen, 1949). However, the ~50–100  $\mu$ m thick central region for nanoindentation test was not ossified up to 24 weeks of age.

### 2.2. Atomic force microscopy (AFM)-based nanoindentation

Each meniscus was mounted on a stainless steel AFM disk via cyanoacrylate glue (Pelco Pro C300, Ted Pella, Inc.). Care was taken to ensure that the glue did not cover or infiltrate through the < 1 mm thick meniscus tissue, as later on confirmed by scanning electron microscope (SEM) images. For each meniscus, AFM-based nanoindentation was performed on the surface of the central, non-ossified region using a microspherical probe tip and a Dimension Icon AFM (BrukerNano, Santa Barbara, CA) (Fig. 1b). The spherical tip was prepared by attaching a borosilicate colloid ( $R_{tip}=5.3 \pm 0.4 \mu$ m, mean  $\pm$  STD on  $n=120$  colloids measured via optical microscope, Polysciences, Warrington, PA) onto the tipless cantilever (nominal spring constant  $k \approx 7.4$  N/m, AIO-TL tip C, NanoAndMore, Lady's Island, SC) using the M-Bond 610 epoxy (Polysciences) under the Dimension Icon AFM. For each meniscus, at least 10 different locations were tested up to an indentation depth of  $\approx 0.3 \mu$ m at 10  $\mu$ m/s rates. In addition, to study the rate-dependent mechanical properties of murine meniscus, for 8-week old murine menisci, indentation was repeated with 0.316–10  $\mu$ m/s rates at each location. Each nanoindentation was found to result in negligible irreversible plastic deformation of the tissue, as suggested by the high repeatability of indentation curves at the same location and same indentation rate. Furthermore, to directly compare to the mechanical properties of murine articular cartilage, nanoindentation was also performed on the right

hind knee medial condyle articular cartilage of 12-week old male mice at 10  $\mu$ m/s indentation depth rate, following previously established procedures (Batista et al., 2014). During all the indentation measurements, meniscus and cartilage tissues were immersed in 0.15 M PBS (pH=7.4) with protease inhibitors (Pierce) to maintain the physiological-like fluid environment.

### 2.3. Indentation data analysis

Each indentation force versus depth,  $F$ - $D$ , curve was analyzed by two methods (Fig. 1c). First, following our previous established procedure on articular cartilage (Han et al., 2011), we calculated the effective indentation modulus,  $E_{ind}$ , at each rate by fitting the entire portion of each loading  $F$ - $D$  curve with Hertz model via least squares linear regression (LSLR)

$$F = \frac{4}{3} \frac{E_{ind}}{(1-\nu^2)} R_{tip}^{1/2} D^{3/2} \quad (1)$$

where  $R_{tip}$  is the tip radius ( $\approx 5 \mu$ m), and  $\nu$  is the Poisson's ratio ( $\approx 0$  for meniscus). The choice of Poisson's ratio was based on the estimate from tissue-level studies on other species (Sweigart et al., 2004). However, varying  $\nu$  from 0–0.5 only yielded  $\approx 25\%$  difference in calculated  $E_{ind}$ , and did not affect the conclusions of this study.

Secondly, for each  $F$ - $D$  curve, we calculated the effective indentation stiffness,  $S_{ind}$ , as the slope of the entire portion of the loading curve via LSLR

$$S_{ind} = \frac{dF}{dD} \quad (2)$$

The coefficient of determination,  $R^2$ , was used to compare the goodness-of-fit by these two methods. For all the  $F$ - $D$  curves, the tip-sample adhesion forces were found to be negligible compared to the indentation forces ( $\sim 1 \mu$ N, Fig. 1c).

### 2.4. Scanning electron microscopy (SEM) and tapping mode AFM imaging

To qualitatively interpret the biomechanical properties of murine meniscus in the context of its matrix collagen structure, serial enzymatic digestions were carried out to enable direct visualization of collagen fibrils on the surface of 12-week old murine menisci. Immediately after nanoindentation, menisci was incubated in 0.1 mg/mL bovine pancreatic trypsin (Sigma-Aldrich, St. Louis, MO) in PBS (pH=7.4) at 37 °C for 24 h to remove proteoglycans, as previously described (Rojas et al., 2014). Tissues were then incubated in 0.4 U/mL hyaluronidase (Sigma-Aldrich) in PBS with 10 mM sodium acetate (pH=6.0) at 37 °C for 24 h to remove hyaluronan (Vanden Berg-Foels et al., 2012). After the digestion, samples were fixed with Karnovsky's fixative (Electron Microscopy Sciences, Hatfield, PA) for 3 h at room temperature, and then rinsed thoroughly with deionized water to remove chemical residuals. The samples were first dehydrated in a series of graded ethanol-water mixtures (ethanol volume ratio: 25%, 50%, 75%, 80% and 100%), each for two 10 min immersions. They were then immersed in a series of graded mixtures of hexamethyldisilazane (HMDS) (Sigma-Aldrich) and ethanol (HMDS volume ratio: 25%, 50%, 75% and 100%), each for two 10 min immersions (Bray et al., 1993). As surface tension was minimized in HMDS, the samples were dried in air overnight to retain the 3D architecture of the collagen structure and stored in a desiccator prior to imaging.

For tapping mode AFM imaging, a nanosized, pyramidal AFM tip (nominal  $R_{tip} \approx 10$  nm, nominal  $k \approx 42$  N/m, NCHV, BrukerNano) was used to visualize the meniscus surface collagen fibril architecture ( $n=3$  medial menisci at 12 weeks of age) in ambient conditions using the Dimension Icon AFM. For SEM imaging, additional samples ( $n=3$  medial menisci at 12 weeks of age) were thermally coated with 10 nm platinum, and imaged immediately via SEM (Supra 50vp, Zeiss, Peabody, MA). For both SEM and AFM images, the distributions of collagen diameter and alignment angle,  $\theta$ , with respect to the circumferential direction were manually measured via ImageJ.

### 2.5. Statistical analysis

Non-parametric statistical tests were used to avoid the assumption of normal distribution. Mann-Whitney U test was performed on the average  $S_{ind}$ , or  $E_{ind}$ , of menisci from each mouse to detect whether  $S_{ind}$  or  $E_{ind}$  vary significantly between the lateral versus medial compartments, or vary between meniscus and cartilage. Kruskal-Wallis test was performed to detect the variations with respect to indentation regions (inner, middle and outer), and mouse age. Friedman test was performed to examine the rate dependence of  $E_{ind}$  or  $S_{ind}$ . To compare the linear fit versus Hertz model, Wilcoxon signed-rank test was performed on the average coefficient of determination,  $R^2$ , obtained on each mouse with both fits. Except for those presented in Fig. 2b, data obtained on one mouse were pooled, as no significant differences were found between left versus right meniscus, or between medial versus lateral compartments. In all the tests, a  $p$ -value of less than 0.05 was taken as statistically significant.



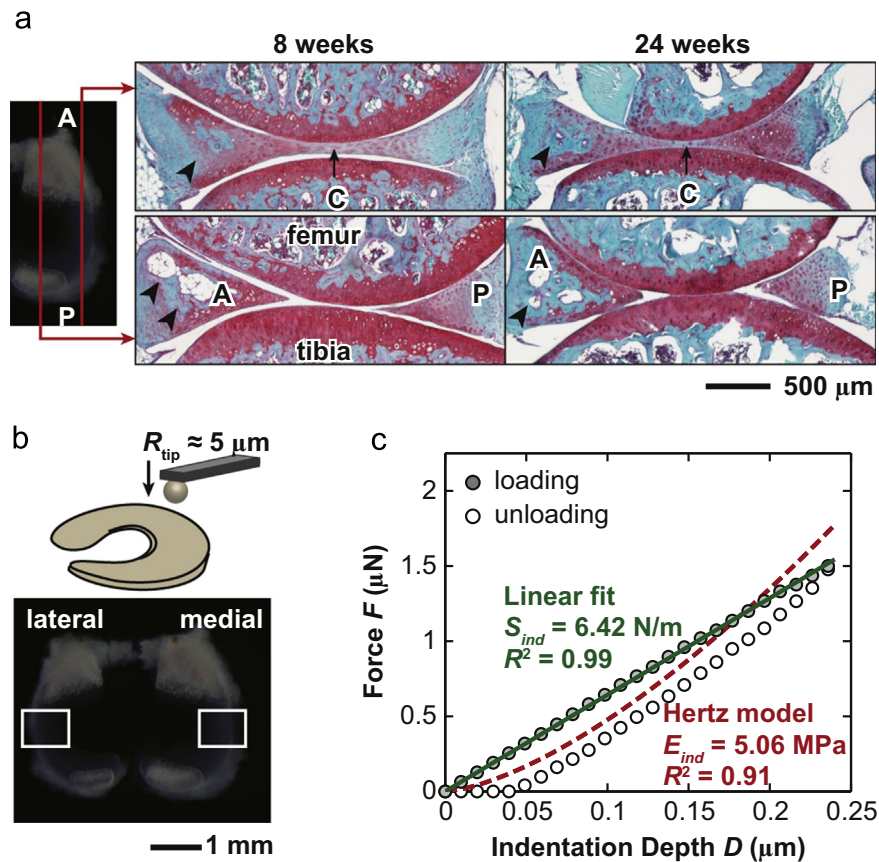


**Fig. 1.** AFM-based nanoindentation of murine meniscus surface. (a) Safranin-O/FastGreen histological staining of the sagittal cross-section of the medial compartments from 8- and 24-week old murine knees. Increased ossification at the anterior (A) and posterior (P) horns with age was shown as white-to-blue staining (black arrowheads). The  $\sim 50$ – $100$   $\mu\text{m}$  thick central region (C) for nanoindentation test was not ossified. (b) Schematic of AFM-based nanoindentation on murine meniscus, where the two squares highlight the regions of interest, i.e., the proximal side, central region of each meniscus surface. (c) Typical indentation force versus depth ( $F$ – $D$ ) curve on one 8-week old murine medial meniscus at  $10$   $\mu\text{m/s}$  indentation depth rate. The linear fit on the loading curve yields higher coefficient of determination,  $R^2$ , than the Hertz model. (For interpretation of the references to color in this figure legend, the reader is referred to the web version of this article.)

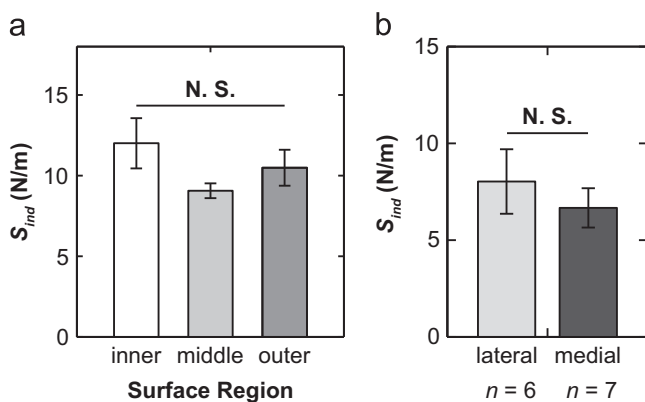


**Fig. 2.** Absence of mechanical heterogeneity across different anatomical sites. (a) Effective indentation stiffness,  $S_{ind}$ , showed no significant difference within the inner, middle and outer surface regions, measured on the meniscus central region of one 6-week old mouse (mean  $\pm$  SEM of  $\geq 8$  locations in each region,  $p > 0.05$  via Kruskal–Wallis test). (b)  $S_{ind}$  of lateral versus medial menisci showed no significant difference (mean  $\pm$  SEM of the average  $S_{ind}$  measured on each 12-week old meniscus,  $n=6$  for lateral and  $n=7$  for medial menisci,  $p > 0.05$  via Mann–Whitney U test). All the values were measured at  $10$   $\mu\text{m/s}$  indentation depth rate.

### 3. Results

For all menisci, most indents yielded a unique, non-Hertzian indentation response. The  $F$ – $D$  curves were found to behave more linearly at all tested rates, rather than the typical  $F$ – $D^{3/2}$  Hertzian pattern (Fig. 1c). For each  $F$ – $D$  curve,  $S_{ind}$  was calculated to provide

a more precise description of the  $F$ – $D$  dependence. The Hertz model-based  $E_{ind}$  was also calculated to enable direct comparison with the moduli of menisci in other species, and with those of murine articular cartilage.

We did not find significant heterogeneity across different anatomical locations. On the proximal side of each meniscus,  $S_{ind}$  was found not to vary significantly across the inner, middle and outer regions (Fig. 2a). We therefore pooled the data obtained at all three regions from each meniscus. In addition, absence of significance in  $S_{ind}$  was found between the lateral and medial menisci (Fig. 2b). Similar to other soft tissues, significant rate dependence was detected here, where increasing indentation rate from  $0.316$  to  $10$   $\mu\text{m/s}$  significantly increased  $S_{ind}$ . Furthermore, the linear  $F$ – $D$  behaviors were persistent at all the tested rates (Fig. 3).

Within the tested murine age from 6 to 24 weeks, we did not find significant trend in  $S_{ind}$  (or  $E_{ind}$ ).  $S_{ind}$  was found to be  $9.6 \pm 1.0$  N/m,  $7.8 \pm 1.0$  N/m,  $7.3 \pm 0.9$  N/m and  $7.5 \pm 1.0$  N/m at 6, 8, 12 and 24 weeks of age, respectively (Fig. 4a). When the Hertz model was applied,  $E_{ind}$  was  $9.2 \pm 1.6$  MPa,  $6.7 \pm 1.1$  MPa,  $6.1 \pm 0.8$  MPa and  $7.0 \pm 1.2$  MPa, at 6, 8, 12 and 24 weeks of age, respectively (Fig. 4b). In all tested ages, the coefficient of determination in LSLR,  $R^2$ , was significantly higher when using the linear fit than using the Hertz model (Fig. 4c). When compared to its direct contact counterpart, the articular cartilage surface, the murine meniscus surface appeared much stiffer. As shown in Fig. 5, nanoindentation on 12-week old murine cartilage yielded  $E_{ind}$  of  $1.4 \pm 0.1$  MPa,  $\approx 4 \times$  lower than the moduli of meniscus at the same age.

Results from tapping mode AFM and SEM imaging on 12-week old meniscus surfaces were consistent ( $p > 0.05$  via Mann-Whitney test), and were therefore pooled for analysis. The images yielded unique structural features of murine meniscus surface. Unlike the human tissues, we found the majority of surface collagen fibrils are aligned nearly along the circumferential direction as fibril bundles (Fig. 6a–c). The diameters of collagen fibrils were found to be  $49.8 \pm 9.5$  nm (mean  $\pm$  STD of 325 fibrils on the medial menisci of six 12-week old mice, 232 from SEM and 93 from AFM, Fig. 6d), similar to those of C57BL/6 wild-type murine articular cartilage surface (Batista et al., 2014). In addition, the absolute values of the angle of each fibril alignment with respect to the circumferential direction,  $\theta$ , were found to be  $21.9 \pm 20.7^\circ$  (429 fibrils on six 12-week old mice, 324 from SEM and 105 from AFM, Fig. 6e). The median of  $\theta$  was  $15.0^\circ$ . As shown by the distribution of  $\theta$ , in addition the dominance of circumferentially aligned fibril bundles, there also existed transversely aligned fibrils interdigitating throughout these circumferential fibril bundles (e.g., white arrowheads in Fig. 6b and c), with a marginal preferential alignment along the radial direction (e.g.,  $3.7 \pm 0.9\%$  of fibrils at  $70^\circ \leq \theta < 80^\circ$ , Fig. 6e).

## 4. Discussion

### 4.1. Non-Hertzian indentation responses of murine meniscus surface

The linear  $F$ - $D$  indentation response of murine meniscus surface is reported here for the first time (Figs. 1c, 3 and 5). This non-Hertzian behavior likely originates from the densely packed, highly anisotropic collagen fibril structure of the meniscus surface

(Fig. 6). As revealed by SEM and AFM imaging on the 12-week old menisci, the surface is dominated by densely packed, circumferentially aligned fibril bundles, interdigitated by sparsely distributed, transversely aligned fibrils (white arrowheads in Fig. 6b and c). This structure leads to substantial tension–compression asymmetry. When nanoindentation was performed normal to the surface, forces could mainly originate from the fibril tension resistance. In such highly aligned, densely packed fibril bundles, when fibril stretching, rather than uncrimping/realignment, dominates its deformation, stresses can travel along the fibrils much further beyond the local contact region (Wang et al., 2014). In this experiment, stresses likely transmit along the fibril bundles to a distance orders of magnitude ( $\gg 10$   $\mu\text{m}$ ) greater than the tip-sample contact radius ( $\approx 2.2$   $\mu\text{m}$  at  $0.5$   $\mu\text{m}$  indentation depth). As a result, stresses were not localized, and indentation forces may not directly scale with the tip-sample contact area, as would be predicted by the Hertz model.

Another possible origin of this non-Hertzian response is the time-dependent poroviscoelasticity. It has been shown that when the indentation time is comparable with the characteristic viscoelasticity time ( $t_{\text{indent}}/\tau_{\text{visco}} \sim 1$ ),  $F$ - $D$  curves measured by a spherical tip follows a linear pattern (Sakai, 2002). However, we observed the linear  $F$ - $D$  curves at all indentation rates (0.316–10  $\mu\text{m/s}$ , Fig. 3a), rather than at one particular rate. While the rate dependent indentation behavior was only reported for 8-week old menisci (Fig. 3), this linear  $F$ - $D$  relationship was found to persist at other ages (6–24 weeks) in the range of 0.1–10  $\mu\text{m/s}$  indentation rates as well (data not shown). Thus, it is less likely

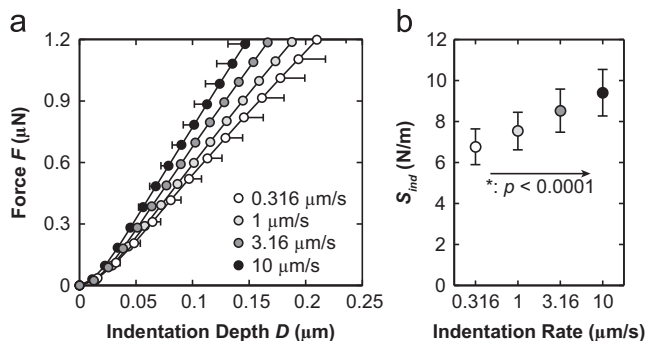


**Fig. 3.** Indentation rate-dependent mechanical properties of murine meniscus surface. (a) Indentation force versus depth curves at 0.316–10  $\mu\text{m/s}$  indentation depth rates. (b) Significant rate dependence of  $S_{\text{ind}}$  was detected via Friedman's test ( $p < 0.0001$ ). For both panels, data shown are mean  $\pm$  SEM of  $\geq 8$  locations on one 8-week old medial meniscus.

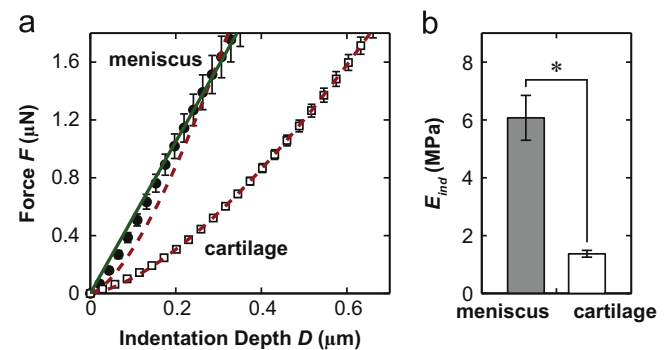


**Fig. 5.** Comparison of the mechanical properties between murine meniscus and cartilage surfaces. (a) Typical indentation  $F$ - $D$  curves on the one medial meniscus and medial condyle cartilage (mean  $\pm$  SEM of  $\geq 10$  positions each, 12 weeks age). The green solid line is the linear fit for meniscus data, and red dashed lines are Hertzian fits for both. (b) Meniscus surfaces ( $n=13$ ) showed significantly higher  $E_{\text{ind}}$  than articular cartilage surfaces ( $n=6$ ) at 12 weeks age (\*:  $p < 0.0001$  via Mann-Whitney U test). All the data were measured at 10  $\mu\text{m/s}$  indentation depth rate. (For interpretation of the references to color in this figure legend, the reader is referred to the web version of this article.)

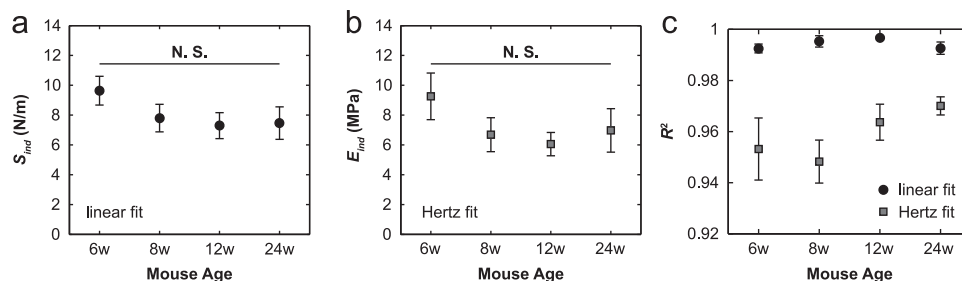


**Fig. 4.** Mechanical properties of murine meniscus surface at different ages. (a, b) Effective indentation stiffness,  $S_{\text{ind}}$  (a), and modulus,  $E_{\text{ind}}$  (b), of the proximal side meniscus surface at 6 weeks ( $n=5$ ), 8 weeks ( $n=10$ ), 12 weeks ( $n=13$ ) and 24 weeks ( $n=5$ ) of ages showed no significant age dependence ( $p > 0.05$  via Kruskal-Wallis test). (c) Comparison of coefficient of determination,  $R^2$ , calculated via the fits of  $S_{\text{ind}}$  and  $E_{\text{ind}}$ . The linear fit yields significantly higher  $R^2$  than the Hertz model ( $p < 0.0001$  via Wilcoxon signed rank test). For all three panels, data shown are mean  $\pm$  SEM of the average values measured on meniscus at the given age cohort at 10  $\mu\text{m/s}$  indentation depth rate.

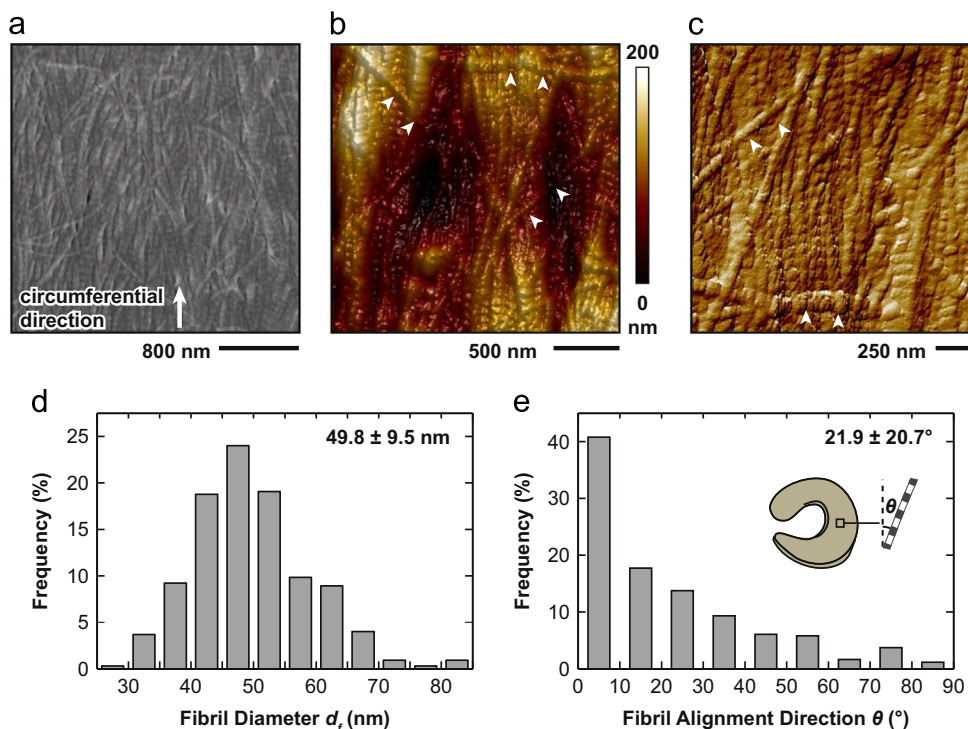


**Fig. 6.** Collagen architecture of murine meniscus surface. Typical (a) SEM and tapping mode AFM (b) height and (c) amplitude images at different scales show that collagen fibrils are mostly aligned as bundles along the circumferential direction on meniscus surface, interdigitated by transversely aligned fibrils (white arrowheads in b). (d, e) Histograms of (d) collagen diameter and (e) collagen alignment with respect to the circumferential direction, respectively. Values reported are mean  $\pm$  STD of 325 fibrils for diameter (232 from SEM, 93 from AFM), and 429 fibrils for alignment direction (324 from SEM, 105 from AFM) from six 12-week old medial menisci.

that poroviscoelasticity is the dominating factor. We hypothesize that the tension resistance of meniscus surface collagen fibrils is the main factor of this non-Hertzian  $F$ - $D$  response, while poroviscoelastic time-dependence may play a minor role. Current studies are aimed at quantitatively investigating the origins of this non-Hertzian response by combining AFM imaging, AFM-nanoindentation at different length scales and fibril-reinforce finite element models (Soulhat et al., 1999) to quantitatively reveal the nanostructure-nanomechanics relationships of murine meniscus and the associated age-dependence.

#### 4.2. Absence of anatomical location dependence

We did not observe significant variations in  $S_{ind}$  (or  $E_{ind}$ ) across the inner to outer regions on each meniscus (Fig. 2a), or between the lateral versus medial menisci (Fig. 2b). This lack of mechanical heterogeneity may be associated with the unique biomechanical functions of the meniscus surface. These functions include load distribution and transmission with cartilage, and the maintenance of meniscus tissue structural integrity (Andriacchi et al., 2004; Walker and Erkman, 1975). A structurally more homogeneous surface layer could be more effective in distributing stress to the interior and may reduce the risk of meniscus tear. This phenomenon of homogeneity is consistent with previous studies on the instantaneous modulus of skeletally mature porcine meniscus measured by AFM-nanoindentation (Sanchez-Adams et al., 2013), and local tissue strain distribution of young bovine menisci via depth-dependent strain monitoring (Lai and Levenston, 2010). Interestingly, this relative homogeneity of the surface is in high contrast to the salient heterogeneity of the interior meniscus. Different regions in the meniscus interior are known to have distinctive mechanical functions. As shown previously for porcine menisci, the outer (red) zone that mainly sustains circumferential tensile stresses is mechanically distinct from the inner (white)

zone (Sanchez-Adams et al., 2013) that mostly undergoes compression (Makris et al., 2011).

#### 4.3. Absence of age-dependence

We also did not observe significant age-dependence in  $S_{ind}$  or  $E_{ind}$  from young, immature (6 weeks) to mature (24 weeks) mice (Fig. 4). This lack of age-dependence could be attributed to the dominance of type I collagen-based fibrils and negligible concentration of proteoglycan content on meniscus surface (Moyer et al., 2013), as the turnover of collagen is known to be markedly longer than other matrix constituents. For example, in human femoral head cartilage, the metabolic half-life of type II-dominated collagen is  $\approx 117$  years (Verzijl et al., 2000), while that of aggrecan is  $\approx 3.4$  years (Maroudas et al., 1998). In human skin, the half-life of type I-dominated collagen is  $\approx 15$  years (Verzijl et al., 2000). The half-life of murine meniscus collagen has not been quantified. However, it is reasonable to expect a collagen network half-life comparable to the life expectancy of mice, or at least, to the age span (6 to 24 weeks) of this study. It is therefore likely that meniscus structure and mechanics exhibit much less age-dependent variations within the tested age than the aggrecan-rich cartilage. Interestingly, while we did not find significant age dependence in meniscus (Fig. 4), the density and modulus of cortical bone from the same C57BL/6 mouse strain was found to significantly increase with age within 4 to 24 weeks of age. However, this increase in modulus was marginal after 8 weeks of age, and was highly correlated with increase in the degree of mineralization (Somerville et al., 2004). For the central region of meniscus, in the absence of mineralization, the temporal trend of development and maturation could be different from that of cortical bone. We believe that future studies targeted to younger and older mice can further elucidate the mechanical implications of meniscus, as well as its association with skeletal development and aging.



#### 4.4. Comparison to meniscus of other species

Interestingly, the murine meniscus surface showed significantly higher  $E_{ind}$  than those of other species measured via nano-indentations. In this study,  $E_{ind}$  of 12-week old menisci was  $6.1 \pm 0.8$  MPa (Fig. 3b). In comparison, for skeletally mature porcine meniscus surface, AFM-based nanoindentation with an  $R_{tip} \approx 2.5$   $\mu$ m spherical tip showed moduli in the range of  $36 \pm 7$  kPa (reported as mean  $\pm$  SD, outer zone) to  $60 \pm 15$  kPa (inner zone) (Sanchez-Adams et al., 2013). For human meniscus surface, instrumented microindentation with an  $R_{tip} \approx 150$   $\mu$ m spherical tip showed steady state modulus of  $1.65 \pm 0.13$  MPa for 57–70 years old tissues (Moyer et al., 2012). This markedly higher  $E_{ind}$  of murine meniscus is likely associated with their smaller body weight than other species. Recently, a negative allometric scaling was found between articular cartilage thickness and body mass across many species, including mouse, human and others. This relation was hypothesized to contribute to a decrease in cartilage biomechanical properties as increasing body weight (Malda et al., 2013). This hypothesis was supported by our previous nanoindentation work on wild-type murine knee cartilage, where murine cartilage was found to be significantly stiffer ( $E_{ind} \sim 1$  MPa) (Batista et al., 2014) than cartilage of larger species, including porcine (McLeod et al., 2013), bovine (Nia et al., 2011) and human (Stolz et al., 2009) tissues ( $E_{ind} \sim 0.1$  MPa). For meniscus, there has been no systematic study on the relationship between body mass and tissue size across species. However, since the thickness of meniscus is similar to articular cartilage in both mouse ( $\sim 50$ – $100$   $\mu$ m in the central region, Fig. 1a) and human ( $\sim 2$  mm; Wenger et al., 2013), it is likely that similar allometric scaling law is also present. As supported by recent tissue-level studies (Joshi et al., 1995; Sweigart et al., 2004), macroindentation measurements found that the smaller lapine menisci had significantly higher aggregate moduli than the larger human, porcine and bovine tissues (Sweigart et al., 2004).

#### 4.5. Comparison to murine articular cartilage

The moduli of murine meniscus surface were significantly higher than its direct contact counterpart, the articular cartilage ( $E_{ind} = 1.4 \pm 0.1$  MPa, Fig. 5b). In addition, as shown in this and previous (Batista et al., 2014) studies, indentation of articular cartilage resulted in typical Hertzian-like  $F$ – $D$  curves (Fig. 5a). The surface layer of articular cartilage is mostly composed of transversely aligned, type II-dominated collagen fibrils, with higher proteoglycan concentrations than meniscus (Xia et al., 2008). The lower cartilage moduli are likely associated with the less organized, less densely packed, or less pre-stretched collagen fibril networks on the surface. In comparison to meniscus, the presence of abundant proteoglycans in articular cartilage may also contribute to the stress localization and higher degree of isotropy, and thus, lead to more Hertzian-like indentation responses.

#### 4.6. Implications for murine model-based osteoarthritis studies

Mechanical knowledge obtained in this study can be applied to murine-based osteoarthritis studies. Recently, AFM-based nano-mechanical tests on murine cartilage have become a valuable tool for investigating the articular cartilage biomechanical function and pathogenesis of OA (Batista et al., 2014; Nia et al., 2015; Stolz et al., 2009; Willard et al., 2014). Successful execution of AFM-based nanoindentation on murine cartilage demonstrated the potential of using similar approaches to provide valuable insights into the roles of meniscus in the development of OA. While OA is now recognized as a whole-joint disease (Poole, 2012), understanding of the function of meniscus and its interaction with articular

cartilage during OA progression is very limited. A biomechanical focus on murine meniscus can thus provide a novel platform for investigating individual mechanical changes of joint tissues that occur and result in OA. For example, it is suggested that in articular cartilage, OA initiates from superficial layer before propagating to the interior (Saarakkala et al., 2010), while the propagation pattern of OA in meniscus is unclear (Pauli et al., 2011). Based on the knowledge of healthy, normal mice, future studies on the concomitant mechanical changes at the meniscus–cartilage contact interfaces may be used as a novel biomarker for the detection and evaluation of OA when combined with clinically relevant OA models, such as the destabilization of the medial meniscus surgery (Glasson et al., 2007).

## 5. Conclusions

In this study, we quantified the nanomechanical properties of murine meniscus surface via AFM-based nanoindentation. A non-Hertzian, linear  $F$ – $D$  indentation response was detected on normal, healthy murine meniscus surface at 6–24 weeks age. This behavior is likely associated with the highly anisotropic, circumferential collagen fibril bundle-dominated architecture. The indentation modulus/stiffness showed negligible dependence on tested anatomical locations or mouse age. In addition, murine menisci were found to be  $\approx 4 \times$  stiffer than murine articular cartilage. To our knowledge, this is the first study that focused on the mechanical properties of murine meniscus. It is hoped that the knowledge obtained here can lay the ground for future explorations of meniscus developmental biology and OA pathology using transgenic or surgery-induced OA models.

## Conflict of interest statement

The authors of this study have no personal or financial conflicts of interest with this work. All authors were fully involved in the study and preparation of this manuscript and the material within has not been and will not be submitted for publication elsewhere.

## Acknowledgments

This work was supported by the Faculty Start-up Grant at Drexel University (LH), the National Institutes of Health (Grants AR063905 to VR, AR060991 to LQ and AR033236 to CO and AJG). We also thank Dr. R. L. Mauck, Dr. L. J. Soslowsky and Dr. V. B. Shenoy for valuable discussions.


## References

- Amey, L.G., Young, M.F., 2006. Animal models of osteoarthritis: lessons learned while seeking the 'Holy Grail'. *Curr. Opin. Rheumatol.* 18, 537–547.
- Andriacchi, T.P., Mündermann, A., Smith, R.L., Alexander, E.J., Dyrby, C.O., Koo, S., 2004. A framework for the in vivo pathomechanics of osteoarthritis at the knee. *Ann. Biomed. Eng.* 32, 447–457.
- Aspden, R.M., Yarker, Y.E., Hukins, D.W.L., 1985. Collagen orientations in the meniscus of the knee joint. *J. Anat.* 140, 371–380.
- Baro, V.J., Bonnevill, E.D., Lai, X., Price, C., Burris, D.L., Wang, L., 2012. Functional characterization of normal and degraded bovine meniscus: rate-dependent indentation and friction studies. *Bone* 51, 232–240.
- Batista, M.A., Nia, H.T., Önerfjord, P., Cox, K.A., Ortiz, C., Grodzinsky, A.J., Heinegård, D., Han, L., 2014. Nanomechanical phenotype of chondroadherin-null murine articular cartilage. *Matrix Biol.* 38, 84–90.
- Bray, D.F., Bagu, J., Koegler, P., 1993. Comparison of hexamethyldisilazane (HMDS), peldri II, and critical-point drying methods for scanning electron-microscopy of biological specimens. *Microsc. Res. Tech.* 26, 489–495.
- Englund, M., 2008. The role of the meniscus in osteoarthritis genesis. *Rheum. Dis. Clin. North Am.* 34, 573–579.
- Fang, H., Beier, F., 2014. Mouse models of osteoarthritis: modelling risk factors and assessing outcomes. *Nat. Rev. Rheumatol.* 10, 413–421.



- Fithian, D.C., Kelly, M.A., Mow, V.C., 1990. Material properties and structure-function-relationships in the menisci. *Clin. Orthop. Relat. Res.* 252, 19–31.
- Glasson, S.S., Blanchet, T.J., Morris, E.A., 2007. The surgical destabilization of the medial meniscus (DMM) model of osteoarthritis in the 129/SvEv mouse. *Osteoarthr. Cartil.* 15, 1061–1069.
- Han, L., Frank, E.H., Greene, J.J., Lee, H.-Y., Hung, H.-H.K., Grodzinsky, A.J., Ortiz, C., 2011. Time-dependent nanomechanics of cartilage. *Biophys. J.* 100, 1846–1854.
- Herwig, J., Egner, E., Buddecke, E., 1984. Chemical changes of human knee joint menisci in various stages of degeneration. *Ann. Rheum. Dis.* 43, 635–640.
- Hunter, D.J., Zhang, Y.Q., Niu, J.B., Tu, X., Amin, S., Clancy, M., Guermazi, A., Grigorian, M., Gale, D., Felson, D.T., 2006. The association of meniscal pathologic changes with cartilage loss in symptomatic knee osteoarthritis. *Arthritis Rheum.* 54, 795–801.
- Joshi, M.D., Suh, J.-K., Marui, T., Woo, S.L.-Y., 1995. Interspecies variation of compressive biomechanical properties of the meniscus. *J. Biomed. Mater. Res.* 29, 823–828.
- Katsuragawa, Y., Saitoh, K., Tanaka, N., Wake, M., Ikeda, Y., Furukawa, H., Tohma, S., Sawabe, M., Ishiyama, M., Yagishita, S., Suzuki, R., Mitomi, H., Fukui, N., 2010. Changes of human menisci in osteoarthritic knee joints. *Osteoarthr. Cartil.* 18, 1133–1143.
- Klompmaier, J., Jansen, H.W.B., Veth, R.P.H., Nielsen, H.K.L., de Groot, J.H., Pennings, A.J., Kuijer, R., 1992. Meniscal repair by fibrocartilage? An experimental study in the dog. *J. Orthop. Res.* 10, 359–370.
- Lai, J.H., Levenston, M.E., 2010. Meniscus and cartilage exhibit distinct intra-tissue strain distributions under unconfined compression. *Osteoarthr. Cartil.* 18, 1291–1299.
- Makris, E.A., Hadidi, P., Athanasiou, K.A., 2011. The knee meniscus: structure-function, pathophysiology, current repair techniques, and prospects for regeneration. *Biomaterials* 32, 7411–7431.
- Malda, J., de Grauw, J.C., Benders, K.E.M., Kik, M.J.L., van de Lest, C.H.A., Creemers, L.B., Dhert, W.J.A., van Weeren, P.R., 2013. Of mice, men and elephants: the relation between articular cartilage thickness and body mass. *PLoS One* 8, e57683.
- Maroudas, A., Bayliss, M.T., Uchitel-Kaushansky, N., Schneiderman, R., Gilav, E., 1998. Aggrecan turnover in human articular cartilage: use of aspartic acid racemization as a marker of molecular age. *Arch. Biochem. Biophys.* 350, 61–71.
- McLeod, M.A., Wilusz, R.E., Guilak, F., 2013. Depth-dependent anisotropy of the micromechanical properties of the extracellular and pericellular matrices of articular cartilage evaluated via atomic force microscopy. *J. Biomech.* 46, 586–592.
- Moyer, J.T., Abraham, A.C., Donahue, T.L.H., 2012. Nanoindentation of human meniscal surfaces. *J. Biomech.* 45, 2230–2235.
- Moyer, J.T., Priest, R., Bouman, T., Abraham, A.C., Donahue, T.L.H., 2013. Indentation properties and glycosaminoglycan content of human menisci in the deep zone. *Acta Biomater.* 9, 6624–6629.
- Nia, H.T., Gauci, S., Azadi, M., Hung, H.-H., Frank, E., Fosang, A.J., Ortiz, C., Grodzinsky, A.J., 2015. High-bandwidth AFM-based rheology is a sensitive indicator of early cartilage aggrecan degradation relevant to mouse models of osteoarthritis. *J. Biomech.* 48, 162–165.
- Nia, H.T., Han, L., Li, Y., Ortiz, C., Grodzinsky, A.J., 2011. Poroelasticity of cartilage at the nanoscale. *Biophys. J.* 101, 2304–2313.
- Pauli, C., Grogan, S.P., Patil, S., Otsuki, S., Hasegawa, A., Koziol, J., Lotz, M.K., D'Lima, D.D., 2011. Macroscopic and histopathologic analysis of human knee menisci in aging and osteoarthritis. *Osteoarthr. Cartil.* 19, 1132–1141.
- Pedersen, H.E., 1949. The ossicles of the semilunar cartilages of rodents. *Anat. Rec.* 105, 1–9.
- Petersen, W., Tillmann, B., 1998. Collagenous fibril texture of the human knee joint menisci. *Anat. Embryol.* 197, 317–324.
- Poole, A.R., 2012. Osteoarthritis as a whole joint disease. *HSSJ* 4, 8–6.
- Proctor, C.S., Schmidt, M.B., Whipple, R.R., Kelly, M.A., Mow, V.C., 1989. Material properties of the normal medial bovine meniscus. *J. Orthop. Res.* 7, 771–782.
- Rojas, F.P., Batista, M.A., Lindburg, C.A., Dean, D., Grodzinsky, A.J., Ortiz, C., Han, L., 2014. Molecular adhesion between cartilage extracellular matrix macromolecules. *Biomacromolecules* 15, 772–780.
- Saarakkala, S., Julkunen, P., Kiviranta, P., Mäkitalo, J., Jurvelin, J.S., Korhonen, R.K., 2010. Depth-wise progression of osteoarthritis in human articular cartilage: investigation of composition, structure and biomechanics. *Osteoarthr. Cartil.* 18, 73–81.
- Sakai, M., 2002. Time-dependent viscoelastic relation between load and penetration for an axisymmetric indenter. *Philos. Mag.* A 82, 1841–1849.
- Sanchez-Adams, J., Wilusz, R.E., Guilak, F., 2013. Atomic force microscopy reveals regional variations in the micromechanical properties of the pericellular and extracellular matrices of the meniscus. *J. Orthop. Res.* 31, 1218–1225.
- Skaggs, D.L., Warden, W.H., Mow, V.C., 1994. Radial tie fibers influence the tensile properties of the bovine medial meniscus. *J. Orthop. Res.* 12, 176–185.
- Somerville, J.M., Aspden, R.M., Armour, K.E., Armour, K.J., Reid, D.M., 2004. Growth of C57BL/6 mice and the material and mechanical properties of cortical bone from the tibia. *Calcif. Tissue Int.* 74, 469–475.
- Soulhat, J., Buschmann, M.D., Shirazi-Adl, A., 1999. A fibril-network-reinforced biphasic model of cartilage in unconfined compression. *J. Biomech. Eng.* 121, 340–347.
- Spilker, R.L., Donzelli, P.S., Mow, V.C., 1992. A transversely isotropic biphasic finite element model of the meniscus. *J. Biomech.* 25, 1027–1045.
- Stolz, M., Gottardi, R., Raiteri, R., Miot, S., Martin, I., Imer, R., Staufner, U., Raducanu, A., Düggelein, M., Baschong, W., Daniels, A.U., Friederich, N.F., Aszodi, A., Aebi, U., 2009. Early detection of aging cartilage and osteoarthritis in mice and patient samples using atomic force microscopy. *Nat. Nanotechnol.* 4, 186–192.
- Sweigart, M.A., Athanasiou, K.A., 2005. Tensile and compressive properties of the medial rabbit meniscus. *Proc. Inst. Mech. Eng. H* 219, 337–347.
- Sweigart, M.A., Zhu, C.F., Burt, D.M., deHoll, P.D., Agrawal, C.M., Clanton, T.O., Athanasiou, K.A., 2004. Intraspaces and interspecies comparison of the compressive properties of the medial meniscus. *Ann. Biomed. Eng.* 32, 1569–1579.
- Vanden Berg-Feels, W.S., Scipioni, L., Huynh, C., Wen, X., 2012. Helium ion microscopy for high-resolution visualization of the articular cartilage collagen network. *J. Microsc.* 246, 168–176.
- Verzijl, N., DeGroot, J., Thorpe, S.R., Bank, R.A., Shaw, J.N., Lyons, T.J., Bijlsma, J.W.J., Lafeber, F.P.J.G., Baynes, J.W., TeKoppele, J.M., 2000. Effect of collagen turnover on the accumulation of advanced glycation end products. *J. Biol. Chem.* 275, 39027–39031.
- Voloshin, A.S., Wosk, J., 1983. Shock absorption of meniscectomized and painful knees: a comparative in vivo study. *J. Biomed. Eng.* 5, 157–161.
- Walker, P.S., Erkman, M.J., 1975. The role of the menisci in force transmission across the knee. *Clin. Orthop. Relat. Res.*, 184–192.
- Wang, H., Abhilash, A.S., Chen, C.S., Wells, R.G., Shenoy, V.B., 2014. Long range force transmission in fibrous matrices enabled by tension-driven alignment of fibers. *Biophys. J.* 107, 2592–2603.
- Wenger, A., Wirth, W., Hudelmaier, M., Noebauer-Huhmann, I., Trattnig, S., Bloecker, K., Frobell, R.B., Kwok, C.K., Eckstein, F., Englund, M., 2013. Meniscus body position, size, and shape in persons with and persons without radiographic knee osteoarthritis: quantitative analyses of knee magnetic resonance images from the osteoarthritis initiative. *Arthritis Rheum.* 65, 1804–1811.
- Willard, V.P., Diekmann, B.O., Sanchez-Adams, J., Christoforou, N., Leong, K.W., Guilak, F., 2014. Use of cartilage derived from murine induced pluripotent stem cells for osteoarthritis drug screening. *Arthritis Rheumatol.* 66, 3062–3072.
- Xia, Y., Zheng, S., Bidthanapally, A., 2008. Depth-dependent profiles of glycosaminoglycans in articular cartilage by  $\mu$ MRI and histochemistry. *J. Magn. Reson. Imaging* 28, 151–157.

# Identification and characterization of adult mouse meniscus stem/progenitor cells

Laura W. Gamer , Rui Rui Shi, Ashira Gendelman, Dylan Mathewson, Jackson Gamer and Vicki Rosen

Department of Developmental Biology, Harvard School of Dental Medicine, Boston, MA, USA

## ABSTRACT

Meniscal damage is a common problem that accelerates the onset of knee osteoarthritis. Stem cell-based tissue engineering treatment approaches have shown promise in preserving meniscal tissue and restoring meniscal function. The purpose of our study was to identify meniscus-derived stem/progenitor cells (MSPCs) from mouse, a model system that allows for *in vivo* analysis of the mechanisms underlying meniscal injury and healing. MSPCs were isolated from murine menisci grown in explant culture and characterized for stem cell properties. Flow cytometry was used to detect the presence of surface antigens related to stem cells, and qRT-PCR was used to examine the gene expression profile of MSPCs. Major proteins associated with MSPCs were localized in the adult mouse knee using immunohistochemistry. Our data show that MSPCs have universal stem cell-like properties including clonogenicity and multi-potentiality. MSPCs expressed the mesenchymal stem cell markers CD44, Sca-1, CD90, and CD73 and when cultured had elevated levels of biglycan and collagen type I, important extracellular matrix components of adult meniscus. MSPC also expressed significant levels of *Lox* and *Igf-1*, genes associated with the embryonic meniscus. Localization studies showed staining for these same proteins in the superficial and outer zones of the adult mouse meniscus, regions thought to harbor endogenous repair cells. MSPCs represent a novel resident stem cell population in the murine meniscus. Analysis of MSPCs in mice will allow for a greater understanding of the cell biology of the meniscus, essential information for enhancing therapeutic strategies for treating knee joint injury and disease.

## ARTICLE HISTORY

Received 22 August 2016  
Revised 5 December 2016  
Accepted 7 December 2016  
Published online 3 February 2017

## KEYWORDS



Mouse meniscus; progenitor cells; stem cells; osteoarthritis

## Introduction


The most common knee injury is damage to the meniscus, a fibrocartilaginous cushion with a pivotal role in protecting the articular cartilages of the tibia and femur from damage during movement. Although treatment of acute meniscal injuries has evolved dramatically in response to an increased understanding of the roles performed by the meniscus within the knee joint, surgical procedures aimed at repairing or replacing damaged menisci are often unsuccessful (1,2). In fact, recent data indicate that surgical repair of meniscal tears cannot reliably prevent the progression of degenerative changes and clinical symptoms that occur post-meniscal injury and presage the development of knee osteoarthritis (OA) (3). Attempts to enhance meniscal healing with addition of fibrin clots or growth factors have shown some promise, consistent with the idea that the intrinsic healing potential of the meniscus might be improved by activation of endogenous meniscal stem cells (4). However, progress in this area has been limited by a lack of information about the origin of meniscal progenitors and the signaling pathways controlling their proliferation and differentiation.

Recently, mesenchymal stem cell (MSC)-based therapies have been used to treat meniscal injuries as an alternative for surgical repair of meniscal lesions. Studies have shown that bone marrow-derived MSCs, adipose-derived MSCs, and synovium-derived MSCs can be used to enhance healing of meniscal defects in animal models (5–10). Although using MSCs has shown promise, tissue-specific stem cells that reside in the meniscus are likely to have distinct characteristics that enable better repair of the meniscus, so that the tissue returns to the fully functional capacity required to prevent joint degeneration (11–13). These include an intrinsic homing capacity that may allow meniscus-derived stem cells to migrate to the injury site (11,14) and the ability to form both chondrogenic and fibrous tissues, a unique feature of this heterogeneous structure (13,15).

A greater understanding of the basic biology of meniscus-derived stem cells will be necessary for their application in cell-based repair and tissue engineering strategies. To this end, we isolated and characterized meniscal stem progenitor cells (MSPCs) from adult mouse meniscus. We chose to analyze murine cells because our data could then

**CONTACT** Laura W. Gamer  [laura\\_gamer@hsdm.harvard.edu](mailto:laura_gamer@hsdm.harvard.edu)  Department of Developmental Biology, Harvard School of Dental Medicine, 188 Longwood Ave, Boston, MA 02115, USA.

Color versions of one or more of the figures in this article can be found online at [www.tandfonline.com/icts](http://www.tandfonline.com/icts).

 Supplemental data for this article can be accessed on the publisher's website.

© 2017 Taylor & Francis

be used to design *in vivo* studies on the regulatory mechanisms underlying meniscal regeneration, as the mouse is an ideal system for genetic manipulation. Mouse MSPCs exhibit the general features of tissue-specific stem cells isolated from other musculoskeletal tissues, including clonogenicity, multi-potency, and expression of several common cell surface markers. In addition, adult mouse MSPCs express meniscus signature genes first identified in embryonic mouse meniscus that may be important for meniscal formation (16). We also show that markers associated with MSPCs localize in distinct regions of the adult mouse meniscus hypothesized to harbor cells capable of responding to meniscal injury, further strengthening the idea that this tissue contains stem/progenitor cells that may be directed toward meniscal repair.

## Materials and methods

### Mice

All mouse studies were approved by the Harvard Medical School Institutional Animal Care and Use Committee. C57Bl/6 mice were obtained from Charles River labs. Mice were maintained in a virus and parasite-free barrier facility and exposed to a 12-hour (h) light/dark cycle.

### Meniscal explant cell isolation and culture

For meniscal explant cultures, hindlimbs were removed from 8-week (wk), 6-month (mo), and 1-year (y)-old mice and placed in a petri dish containing sterile phosphate-buffered saline (PBS) on ice. The surrounding muscle was trimmed away and the knee joint dissected out. The patellar tendon was cut and the femur and tibia separated. The menisci remain attached to the tibia and were removed from the articular surface of the bone using a scalpel and fine curved scissors. The medial and lateral menisci were then placed in sterile PBS on ice. In the tissue culture hood, forceps were used to place 1 pair of menisci into each well of a 6-well plate. One drop (50  $\mu$ l) of growth media consisting of minimum essential medium alpha ascorbic acid free ( $\alpha$ -MEM) (Invitrogen, Carlsbad, CA) supplemented with 20% fetal bovine serum (FBS), 10 mM L-glutamine, 100 units/ml penicillin, and 100  $\mu$ g/ml streptomycin was added to cover each menisci. The plate was incubated for 2 hours at 37°C; 5% CO<sub>2</sub>; 42% humidity to allow the tissue to adhere; and then 1.5 ml of media were added to each well. After 3 days, an additional 1.5 ml of growth media was added and cells began to grow out of the explanted menisci 5–7 days later.

## Colony-forming and multi-differentiation potential assays

For colony-forming efficiency assays, MSPCs from 8-wk-old mice at passage 1 (P1) were cultured at 1000–2000 cells per 25-cm<sup>2</sup> flask in growth media for 12 days and stained with 0.05% methyl violet (Sigma, St. Louis, MO). Only colonies containing more than 50 cells were counted.

For multi-differentiation assays, MSPCs from 8-wk-old mice were plated at colony-forming density (2000 cells) in 25-cm<sup>2</sup> flasks and cultured in growth medium for 12 days. Differentiation media were chosen based on standard protocols for mouse bone marrow stromal cells (17). To analyze osteogenic potential, cells were switched to osteogenic media that consisted of growth media supplemented with 10 mM  $\beta$ -glycerol phosphate and 50  $\mu$ g/ml ascorbic acid (Sigma) for another 7 days. Colonies were then stained with 0.5% alizarin red S (Sigma). To test adipogenic potential, cells were switched to adipogenic media consisting of growth media supplemented with 100 nM dexamethasone, 5  $\mu$ g/ml insulin, and 50  $\mu$ M indomethacin (Sigma) for 7 more days. Colonies were then stained with 0.3% oil red O (Sigma). To assess chondrogenic potential, cells were switched to chondrogenic media consisting of growth media supplemented with 50  $\mu$ g/ml ascorbic acid, 100 nM dexamethasone, 40  $\mu$ g/ml L-proline, 2mM sodium pyruvate, and 1% insulin transferrin-selenious acid mix (ITS+) (Sigma) for another 7 days. Flasks were then stained with alcian blue pH 1.0 (Sigma).

### Flow Cytometry (FACS) analysis

P1 MSPCs from 8-wk-old mice were suspended at a density of  $1 \times 10^6$  cells in FACS buffer (PBS, 1% FBS) containing 1–5  $\mu$ g/ml of primary or control antibodies. After incubation for 30 minutes at 4 °C, the cells were washed three times with FACS buffer and suspended in 500  $\mu$ l FACS buffer for the analysis. The following fluorescein isothiocyanate (FITC), allophycocyanin (APC), or phycoerythrin (PE)-coupled antibodies were used: CD34 (#11-0341; eBiosciences, San Diego, CA), CD44 (#17-0441; eBiosciences), CD73 (#12-0731; eBiosciences), CD105 (#17-1051; eBiosciences), Sca1 (#561077; BD Pharmingen, San Jose, CA), and CD90.2 (#60115FI.2; STEMCELL Technologies, Vancouver, BC). Samples were evaluated using a BDLSRII flow cytometer (BD Biosciences, San Jose, CA), and the data were analyzed using the FlowJo software program (FlowJo, Ashland, OR).

### **RNA isolation and quantitative real-time PCR (qRT-PCR) analysis**

Total RNA was isolated from MSPCs (P1) from 8-wk-old mice using the RNEasy Plus Universal Kit (Qiagen, Valencia, CA). Reverse transcription was performed using EcoDry Premix Kit (Clontech, Mountain View, CA). Quantitative PCR was performed using FastStart Universal SYBR Green Master Mix (Roche, Nutley, NJ) on a StepOnePlus Real-Time PCR System (Applied Biosystems, Life Technologies, Beverly, MA), and primers as outlined in Supplemental Table S1. Values were normalized to *cyclophilin B* using the 2- $\Delta\Delta C_t$  method (18).

### **Immunohistochemistry**

For immunohistochemistry, knees were fixed in 10% neutral-buffered formalin overnight at 4 °C and decalcified for 2 weeks in 0.5M EDTA at 4 °C. Sections of 8-wk-old murine knee joints were deparaffinized, rehydrated, and incubated in citrate buffer pH 6.0 at 65 °C for 1 hr or in hyaluronidase (Sigma) at 37 °C for 10 min for antigen retrieval. Sections were then blocked and incubated with primary antibody overnight at 4 °C. Immunohistochemical detection was performed using a Vectastain ABC kit (Vector Laboratories, Burlingame, CA) according to the manufacturer's instructions and visualized using a DAB peroxidase substrate kit (Vector Laboratories) followed by counterstaining with Hematoxylin QS (Vector Laboratories). Primary antibodies used were biglycan (1:100, Abcam, Cambridge, MA), CD44 (1:1000, Abcam), IGF-1 (1:250 Abcam), and lysyl oxidase (1:250, ThermoFisher, Waltham, MA).

### **Statistical analysis**

Results are presented as the mean plus and minus standard deviation (SD). Data are based on triplicate reactions of at least three biological samples.

## **Results**

### **Mouse meniscal explant culture**

Based on explant culture procedures for human meniscus and cartilage (11,19), a reproducible protocol was developed for isolating meniscal progenitor cells from adult mouse meniscus. After 5–7 days in culture, cells began to grow out of the explanted menisci (Figure 1A). The meniscus-derived cells grew clonally and exhibited a spindle-shaped morphology (Figure 1B) typical of mesenchymal stem cells and similar to migratory meniscal cells from the human meniscus (11). The cells grew equally well out of both the lateral and medial menisci of mice of

all ages tested, were successfully passaged after 14 days, and grew well in monolayer. Subsequent experiments were all performed using meniscal explants from 8-wk-old mice, and the meniscus-derived cells were designated MSPC (meniscal stem progenitor cells).

### **Mouse MSPCs exhibit stem cell-like characteristics**

To begin to characterize the stem cell potential of MSPCs, we examined their clonogenicity. Single-cell suspensions were generated and cultured from 8-wk-old mouse meniscal explants. A portion of these meniscal cells attached onto the plastic surface of the flask and colonies were visualized using methyl violet staining after 12 days (Figure 1C). A small population (2–3%) of the meniscus-derived cells formed adherent colonies that varied in size, cell density, and morphology, reflecting differences in cell proliferation rates and the inherent heterogeneous nature of meniscal tissue (Figure 1D–F).

Next, we examined whether MSPCs had the capacity to differentiate into various cell lineages (osteoblast, adipocyte, chondrocyte), a fundamental characteristic of stem cells. To test the osteogenic potential of this cell population, MSPC colonies were differentiated in osteogenic medium. After 7 days, alizarin red-positive mineralized calcium deposits were detected (Figure 1G). After induction in adipogenic medium for 7 days, MSPC colonies showed accumulation of lipid droplets visualized by positive oil red O staining (Figure 1H). When differentiated in chondrogenic medium for 7 days, MSPC colonies stained positive for alcian blue indicating synthesis of proteoglycans by chondrocytes (Figure 1). These results suggest that MSPCs can form colonies and are multipotential, two key features of mesenchymal stem cells.

### **FACS analysis**

To confirm whether the MSPCs possess the established properties of stem cells, they were subjected to fluorescence-activated cell sorting (FACS) analysis for surface markers associated with stem cells from joint tissues (8,11,13,19–21) (Figure 2A). We found that MSPCs (P1) were over 97% positive for CD44, a mesenchymal stromal cell marker, and over 87% positive for stem cell antigen-1 (Sca-1). In addition, cells were also positive for CD90.2 (54%) and CD73 (35.4%) and expressed low levels of CD105 (2.2%). MSPCs were negative for CD34 verifying the lack of contaminating hematopoietic cells. This flow cytometry profile is similar to that of human migratory meniscus progenitor cells (11) and suggests that mouse MSPCs have characteristics of mesenchymal stem cells.



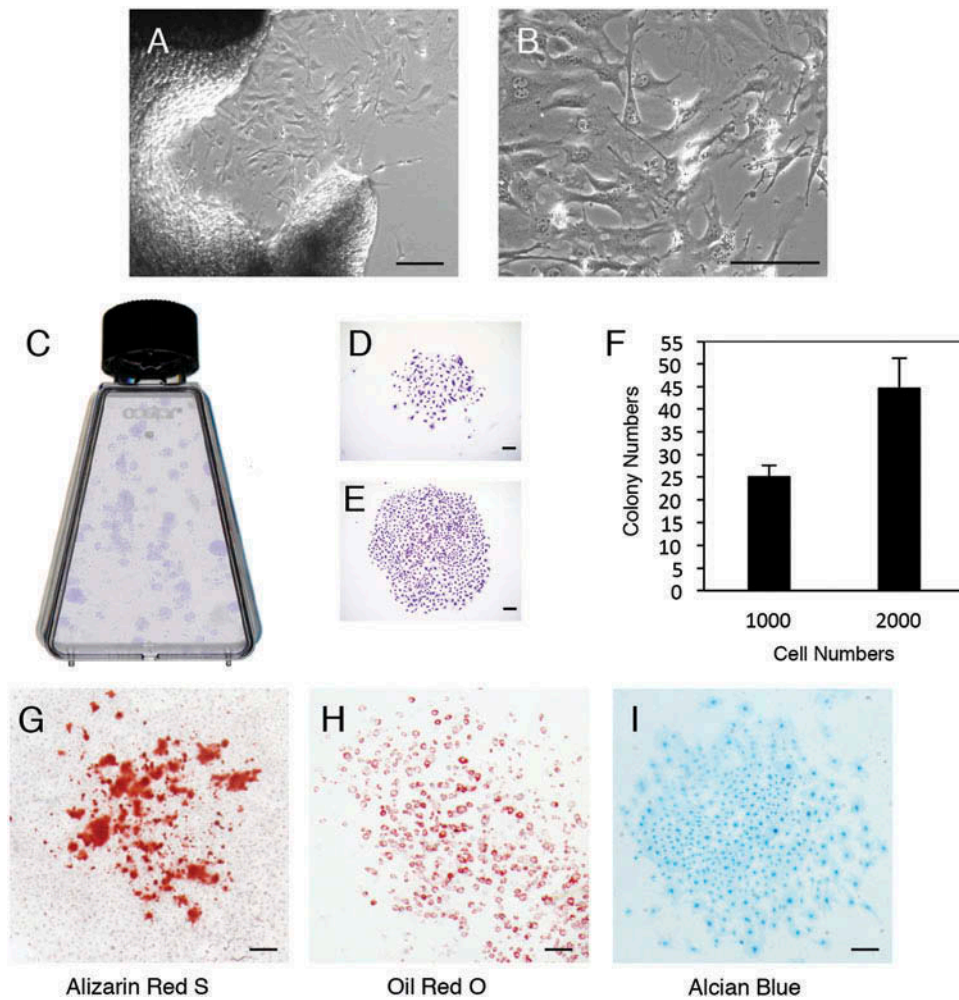


**Figure 1.** Isolation and analysis of stem cell features of MSPCs. (A) Phase contrast microscopy of cells growing out of lateral meniscus of 8-wk-old mouse after 5 days in culture. (B) Higher power view showing the spindle-shaped morphology of these cells. Colony-formation analysis of MSPCs. (C) Colonies formed from 2000 MSPCs after 12 days in culture stained with methyl violet. (D–E) Morphology of sample colonies formed by MSPCs. (F) Colony-forming efficiency of MSPCs. The results are shown as means  $\pm$  SD of three flasks at each cell density. The multi-differentiation potential of MSPCs. (G) Alizarin red S staining shows osteogenic differentiation of MSPCs. (H) Oil red O staining shows adipogenic differentiation of MSPCs. (I) Alcian blue staining shows chondrogenic differentiation of MSPCs. Scale bar = 200  $\mu$ m.

### Gene expression profile of MSPCs

To further characterize the MSPCs, we examined the expression profile of molecular markers of mature meniscus, cartilage, tendon and bone, and also genes we have shown previously to be associated with formation of the embryonic meniscus (16). RNA was isolated from MSPCs expanded to passage 1 (P1) from 8-wk-old mouse meniscal explants. qPCR analysis revealed that MSPCs exhibited high relative expression of *biglycan*, a small leucine-rich proteoglycan found in the meniscus, and *collagen type I*, the major collagen of the outer fibrous region of the meniscus and intermediate levels of *decorin*, the other meniscal small structural proteoglycan, and *Sox9*, a

chondrogenic transcription factor (Figure 2B). In contrast, MSPCs had lower relative expression of the major inner meniscal ECM components *collagen type 2* and *aggrecan* (Figure 2B). This expression pattern may be indicative of the origin of MSPCs from the outer versus the inner region of the meniscus. In addition, MSPCs did not express significant amounts of tendon or bone markers reflecting their potential as tissue-specific progenitor cells for the meniscus (Figure 2B). Intriguingly, MSPCs expressed robust levels of the meniscus signature gene *lysyl oxidase (Lox)*, an enzyme responsible for collagen cross-links in skeletal and connective tissue, as well as *Igf-1*, the major signaling pathway enriched in the developing meniscus (16) (Figure 2C).

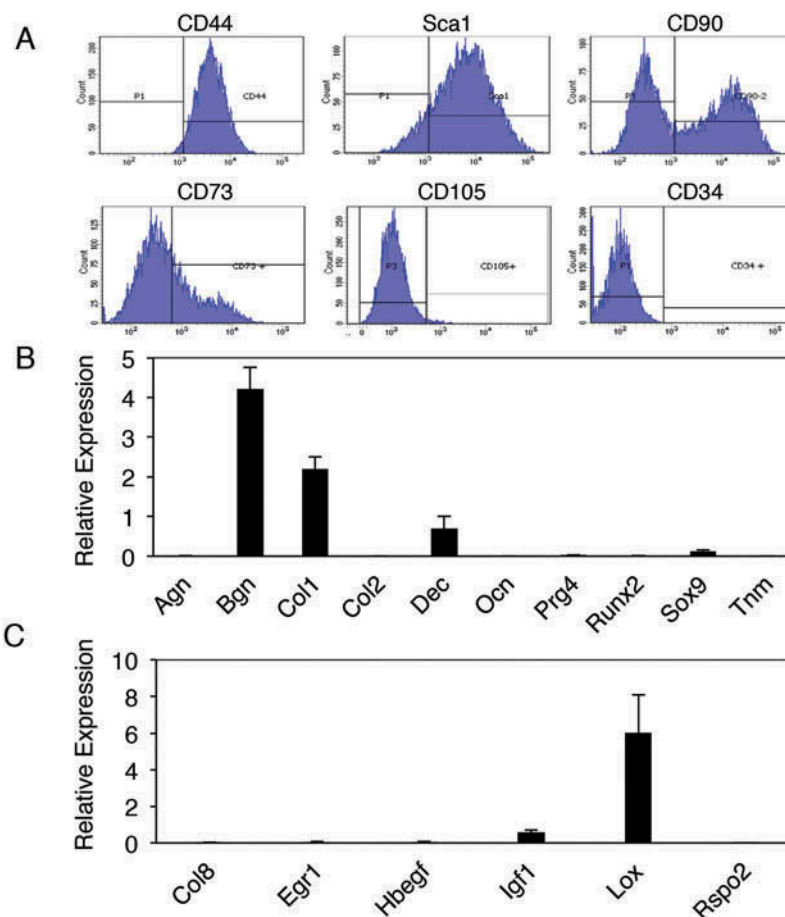


**Figure 2.** Characterization of MSCs. (A) Flow cytometry analysis of the expression of cell surface markers related to stem cells. MSCs were 97.3% positive for CD44, 87.8% positive for Sca-1, 54% positive for CD90, 35.4% positive for CD73, 2.2% positive for CD105, and 0.1% positive for CD34. (B) qRT-PCR analysis for markers of skeletal and connective tissue in MSCs. (C) qRT-PCR analysis of genes associated with embryonic meniscal formation in MSCs. Data represent three biological replicates with *cyclophilin B* used for normalization. Error bars are means  $\pm$  SD.

# Localization of MSCs

Finally, to verify the data obtained from our FACs and qPCR analyses with MSC behavior *in vivo*, we examined the spatial localization of a select group of MSC-expressed factors using immunohistochemistry. CD44, biglycan, Lox, and IGF-1 were all detected in the outer periphery of the meniscus in the fibro-chondrocytes of the superficial zone in knees of 8-wk-old mice (Figure 3A–F). This superficial zone is thought to contain endogenous progenitor cells with regenerative capabilities (22). In addition, positive staining was seen for CD44, biglycan, Lox, and IGF-1 in the fibroblast-like cells of the outer vascular zone. This region is rich in collagen type I and has a higher capacity for healing and repair (15). These data confirm our *in vitro* studies and suggest that in the mouse, endogenous progenitor cells may reside in the superficial and outer region of the meniscus *in vivo*.

# Discussion

A detailed understanding of the molecular and cellular events that underlie tissue repair is essential for addressing pathologies associated with injury, disease, and aging in the musculoskeletal system. Little information exists about resident stem cell populations in the mouse meniscus, a model increasingly used to study joint diseases including OA. Our previous work focused on the developmental biology of mouse meniscus, identifying key events mediating morphogenesis and the signaling pathways that direct this process (16, 23). Here, we report the isolation and characterization of resident meniscus stem/progenitor cells (MSC) derived from adult mouse meniscus explant cultures. MSCs demonstrate general properties of other stem cells including clonogenicity and multipotentiality, express cell surface antigens associated with mesenchymal stem cells, and display elevated levels of meniscal marker genes. In addition, we observe a correlation between sites

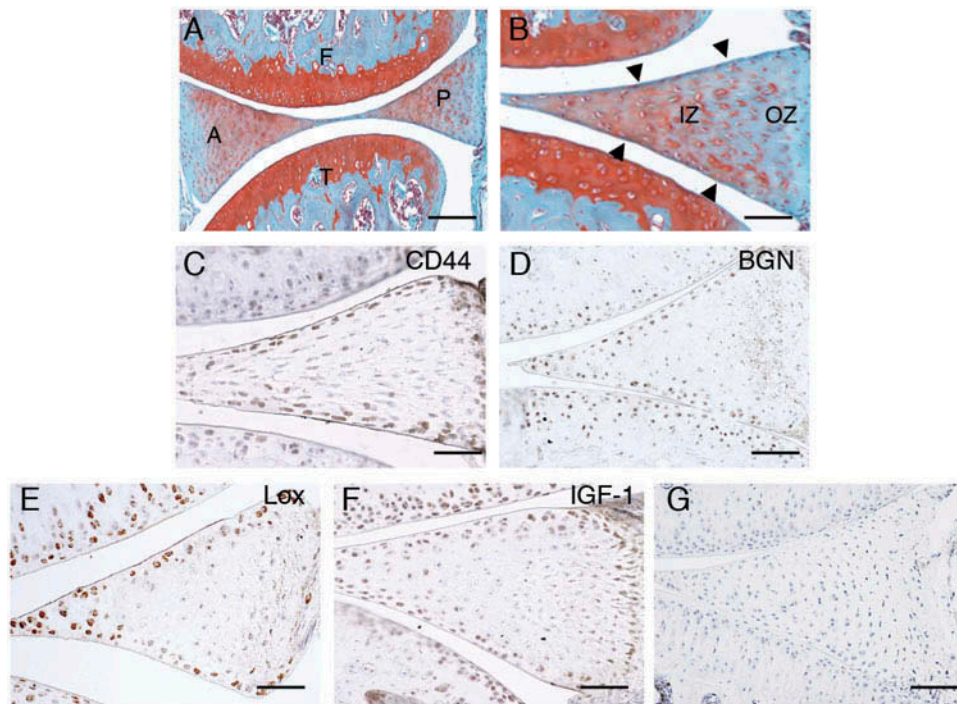


**Figure 3.** Localization of proteins associated with MSCs in mouse knee. (A) Safranin O and fast green staining of 8-wk-old mouse knee (4× magnification). Scale bar = 200 μm. F, femur; T, tibia; A, anterior meniscal horn; P, posterior meniscal horn. (B) High-power view of posterior meniscal horn (10× magnification). Scale bar = 100 μm. Arrowheads point to the superficial zone. IZ, inner zone of meniscus; OZ, outer zone of meniscus. Immunohistochemistry for (C) CD44, (D) biglycan (BGN) (E), lysyl oxidase (Lox), and (F) IGF-1 proteins showed positive staining of cells in the superficial and outer zone of posterior horn of the 8-wk meniscus. (G) No primary antibody negative control stained section. Scale bar = 100 μm.

within the meniscus that are thought to harbor endogenous repair cells and the localization of proteins associated with MSCs. We believe that identification of MSCs provides a powerful tool for enhancing cell-based strategies focused on meniscal regeneration as there is increasing evidence that tissue-resident stem cells are critical for organ homeostasis and effective wound healing (24). Although MSCs and synovium-derived stem cells have been tested in meniscal injury models (5–10), endogenous stem/progenitor cells may be best suited for repair of the meniscus, a tissue with distinct composition, architecture, and function in the knee joint.

In previous studies, meniscus-derived stem cells were identified and isolated from rabbit and human following tissue digestion (12, 13, 21). Unlike those investigations, the MSCs described in our studies migrated out of whole explanted mouse menisci. Since cell motility is now recognized as a vital property of stem and progenitor cells (24), our MSCs may represent a more promising cell population for meniscal repair. The MSCs we identified express progenitor and stem cell markers that localize to the outer vascular zone and superficial zone of the adult meniscus, two areas thought to contain cells for repair (15, 22). As these anatomical sites are distinct in character, the presence of MSCs at both locations suggests the possibility

of multiple stem cell niches within the meniscus. It is also unclear at this point whether our mouse MSCs are a mixed population of stem cells that migrated out of several sites within the meniscus or a single population of MSCs that reside at multiple sites where they respond to specific niche cues. Lineage tracing studies to track cell behavior using transgenic mouse models will be useful in answering this question.

Our *in vitro* analyses of mouse MSC revealed elevated expression levels of *Lox* and *Igf-1*, genes previously identified as highly expressed in embryonic meniscus (16). In the musculoskeletal system, *Lox* functions to covalently cross-link collagen fibers, thus enhancing tissue mechanical integrity. Stimulating endogenous *Lox* expression improves the biomechanical properties of both native and engineered connective tissues, including meniscus (25), so that expression of *Lox* by MSC may be one way of strengthening newly laid down repair tissue. IGF-1 is a critical mediator of both bone and cartilage tissues and has shown promise as a stimulator of cell proliferation and ECM production by meniscal fibrochondrocytes (26, 27). In the context of repair, IGF-1 treatment of engineered meniscal constructs correlates with improved mechanical, biochemical, and surface lubrication properties (28,29). As tissue regeneration



often recapitulates aspects of embryonic tissue morphogenesis, the expression of Lox and IGF-1 by MSPCs may be an identifying characteristic that defines a reparative cell population resident in the adult mouse meniscus.

Overall, our mouse MSPCs had a cell surface marker expression profile similar to meniscal stem cells from rabbit and human and from other tissue sources including synovium, tendon, and fat (7,8,11–13,20,21). The one intriguing exception was CD105 (endoglin), a high affinity co-receptor for TGF- $\beta$ 1, whose expression has traditionally defined mesenchymal stromal cells of adipose and bone marrow origin (30). MSPCs from mouse were only 2% positive for CD105, while MSPCs from rabbit and human were 94–96% positive (11–13). This significant change could be due differences in isolation methods for meniscal stem cells or in the age of the specimen used. For example, the mouse meniscal tissue we used was from healthy 8-wk-old animals, while the human meniscal samples used for MSPCs were from 62- to 75-yr-old patients with late-stage knee OA (11,21). In addition, there may be inherent species variability as the rodent meniscus mineralizes, while the rabbit and human menisci do not (23,31). MSPCs from mouse may need to have low CD105 levels in order to form this bone tissue which is a normal process in their meniscal development and maturation (23,31) as previously reports have shown that low CD105 adipose stem cells have an enhanced capacity for osteogenesis due to decreased TGF- $\beta$ 1/Smad2 signaling (30).

Our current findings support the notion that a greater understanding of the basic biology of meniscal stem/progenitor cells is needed to better inform cell-based treatments for meniscal pathologies. Analysis of meniscus-derived stem cells in an animal model such as the mouse will allow for detailed studies of their behavior during injury and repair and of the regulatory pathways that guide these processes, critical steps in identifying therapeutic targets for the regeneration of diseased or injured meniscal tissue.

## Acknowledgments

We thank the Harvard Medical School System Biology Flow Cytometry Core Facility for expert help with FACs analysis and Nicolae Miosoge and Hyat Muhammad for advice on meniscal explant cultures.

## Declaration of interest

The authors report no conflict of interest. The authors alone are responsible for the content and writing of the article.

## Funding

The research reported in this publication was supported in part by the U.S. Department of Defense under award number W81XWH-13-1-0244 to V.R.

## ORCID

Laura W. Gamer  <http://orcid.org/0000-0002-1324-2741>

## References

1. Petrosini AV, Sherman OH. A historical perspective on meniscal repair. *Clin Sports Med* 1996;15:445–453.
2. Rath E, Richmond JC. The menisci: basic science and advances in treatment. *Br J Sports Med* 2000;34:252–257.
3. Lohmander LS, Englund PM, Dahl LL, Roos EM. The long-term consequence of anterior cruciate ligament and meniscus injuries: osteoarthritis. *Am J Sports Med* 2007;35:1756–17569.
4. Petersen W, Pufe T, Starke C, Fuchs T, Kopf S, Raschke M, Becker R, Tillmann B. Locally applied angiogenic factors: a new therapeutic tool for meniscal repair. *Ann Anat* 2005;187:509–519.
5. Izuta Y, Ochi M, Adachi N, Deie M, Yamasaki T, Shinomiya R. Meniscal repair using bone marrow-derived mesenchymal stem cells: experimental study using green fluorescent protein transgenic rats. *Knee* 2005;12:217–223.
6. Yamasaki T, Deie M, Shinomiya R, Izuta Y, Yasunaga Y, Yanada S, Sharman P, Ochi M. Meniscal regeneration using tissue engineering with a scaffold derived from a rat meniscus and mesenchymal stromal cells derived from rat bone marrow. *J Biomed Mater Res A* 2005;75:23–30.
7. Ruiz-Iban MA, Diaz-Heredia J, Garcia-Gomez I, Gonzalez-Lizan F, Elias-Martin E, Abraira V. The effect of the addition of adipose-derived mesenchymal stem cells to a meniscal repair in the avascular zone: an experimental study in rabbits. *Arthroscopy* 2011;27:1688–1696.
8. Horie M, Sekiya I, Muneta T, Ichinose S, Matsumoto K, Saito H, Murakami T, Kobayashi E. Intra-articular Injected synovial stem cells differentiate into meniscal cells directly and promote meniscal regeneration without mobilization to distant organs in rat massive meniscal defect. *Stem Cells* 2009;27:878–887.
9. Nakagawa Y, Muneta T, Kondo S, Mizuno M, Takakuda K, Ichinose S, Tabuchi T, Koga H, Tsuji K, Sekiya I. Synovial mesenchymal stem cells promote healing after meniscal repair in microminipigs. *Osteoarthritis Cartilage* 2015;23:1007–1017.
10. Kondo S, Muneta T, Nakagawa Y, Koga H, Watanabe T, Tsuji K, Sotome S, Okawa A, Kiuchi S, Ono H, Mizuno M, Sekiya I. Transplantation of autologous synovial mesenchymal stem cells promotes meniscus regeneration in aged primates. *J Orthop Res* 2016. doi:10.1002/jor.23211.
11. Muhammad H, Schminke B, Bode C, Roth M, Albert J, von der Heyde S, Rosen V, Miosge N. Human



- migratory meniscus progenitor cells are controlled via the TGF-beta pathway. *Stem Cell Rep* 2014;3:789–803.
12. Ding Z, Huang H. Mesenchymal stem cells in rabbit meniscus and bone marrow exhibit a similar feature but a heterogeneous multi-differentiation potential: superiority of meniscus as a cell source for meniscus repair. *BMC Musculoskelet Disord* 2015;16:65–78.
  13. Huang H, Wang S, Gui J, Shen H. A study to identify and characterize the stem/progenitor cell in rabbit meniscus. *Cytotechnology* 2016. doi:10.1007/s10616-016-9949-2.
  14. Chevrier A, Nelea M, Hurtig MB, Hoemann CD, Buschmann MD. Meniscus structure in human, sheep, and rabbit for animal models of meniscus repair. *J Orthop Res* 2009;27:1197–1203.
  15. Makris EA, Hadidi P, Athanasiou KA. The knee meniscus: structure-function, pathophysiology, current repair techniques, and prospects for regeneration. *Biomaterials* 2011;32:7411–7431.
  16. Pazin DE, Gamer LW, Capelo LP, Cox KA, Rosen V. Gene signature of the embryonic meniscus. *J Orthop Res* 2014;32:46–53.
  17. Robey PG, Kuznetsov SA, Riminucci M, Bianco P. Bone marrow stromal cell assays: in vitro and in vivo. *Methods Mol Biol* 2014;1130:279–293.
  18. Livak KJ, Schmittgen TD. Analysis of relative gene expression data using real-time quantitative PCR and the 2<sup>-ΔΔC<sub>T</sub></sup> method. *Methods* 2001;25:402–408.
  19. Koelling S, Kruegel J, Irmer M, Path JR, Sadowski B, Miro X, Miosge N. Migratory chondrogenic progenitor cells from repair tissue during the later stages of human osteoarthritis. *Cell Stem Cell* 2009;4:324–335.
  20. Bi Y, Ehrichtou D, Kilts TM, Inkson CA, Embree MC, Sonoyama W, Li L, Leet AI, Seo BM, Zhang L, Sontao S, Young MF. Identification of tendon stem/progenitor cells and the role of the extracellular matrix in their niche. *Nat Med* 2007;13:1219–1227.
  21. Segawa Y, Muneta T, Makino H, Nimura A, Mochizuki T, Ju YJ, Ezura Y, Umezawa A, Sekiya I. Mesenchymal stem cells derived from synovium, meniscus, anterior cruciate ligament, and articular chondrocytes share similar gene expression profiles. *J Orthop Res* 2009;27:435–441.
  22. Kambic HE, Futani H, McDevitt CA. Cell, matrix changes and alpha-smooth muscle actin expression in repair of the canine meniscus. *Wound Repair Regen* 2000;8:554–561.
  23. Gamer LW, Xiang L, Li Q, Han L, Rosen V. Formation and maturation of the murine meniscus. *J Orthop Res* 2016;34:S1.
  24. Goichberg P. Current understanding of the pathways involved in adult stem and progenitor cell migration for tissue homeostasis and repair. *Stem Cell Rev* 2016;12:421–437.
  25. Makris EA, Responde DJ, Paschos NK, Hu JC, Athanasiou KA. Developing functional musculoskeletal tissues through hypoxia and lysyl oxidase-induced collagen cross-linking. *Proc Natl Acad Sci USA* 2014;111:4832–4841.
  26. Tumia NS, Johnstone AJ. Regional regenerative potential of meniscal cartilage exposed to recombinant insulin-like growth factor-I in vitro. *J Bone Joint Surg Br* 2004;86:1077–1081.
  27. Stewart K, Pabbruwe M, Dickinson S, Sims T, Hollander AP, Chaudhuri JB. The effect of growth factor treatment on meniscal chondrocyte proliferation and differentiation on polyglycolic acid scaffolds. *Tissue Eng* 2007;13:271–280.
  28. Puetzer JL, Brown BN, Ballyns JJ, Bonassar LJ. The effect of IGF-I on anatomically shaped tissue-engineered menisci. *Tissue Eng Part A* 2013;19:1443–1450.
  29. Bonnevie ED, Puetzer JL, Bonassar LJ. Enhanced boundary lubrication properties of engineered menisci by lubricin localization with insulin-like growth factor I treatment. *J Biomech* 2014;47:2183–2188.
  30. Levi B, Wan DC, Glotzbach JP, Hyun J, Januszyk M, Montoro D, Sorkin M, James AW, Nelson ER, Li S, Quarto N, Lee M, Gurtner GC, Longaker MT. CD105 protein depletion enhances human adipose-derived stromal cell osteogenesis through reduction of transforming growth factor  $\beta$ 1 (TGF- $\beta$ 1) signaling. *J Biol Chem* 2011;286:39497–39509.
  31. Pedersen HE. The ossicles of the semilunar cartilages of rodents. *Anat Rec* 1949;105:1–9.

## Identification and Characterization of Adult Mouse Meniscus Stem/Progenitor Cells

Laura Gamer<sup>1</sup>, Rui Rui Shi<sup>1</sup>, Ashira Gendelman<sup>1</sup>, Dylan Mathewson<sup>1</sup>, Jackson Gamer<sup>1</sup> and Vicki Rosen<sup>1</sup>  
Harvard School of Dental Medicine, Boston, MA<sup>1</sup>

**Disclosures:** Laura Gamer (N), Rui Rui Shi (N), Ashira Gendelman (N), Dylan Mathewson (N), Jackson Gamer (N), Vicki Rosen (N).

**INTRODUCTION:** The most common knee injury is damage to the meniscus, a fibrocartilaginous cushion with a pivotal role in protecting the articular cartilage from damage during movement. Although treatment of acute meniscal injuries has evolved dramatically in recent years, surgical procedures aimed at repairing or replacing damaged menisci are often unsuccessful. In fact, most surgical repair of meniscal tears cannot reliably prevent the progression of degenerative changes and clinical symptoms that presage the development of knee osteoarthritis (OA). Attempts to enhance meniscal healing with addition of fibrin clots or growth factors have shown some promise, consistent with the idea that the intrinsic healing potential of the meniscus might be improved by activation of endogenous meniscal stem cells. However, progress in this area has been limited by a lack of information about the origin of meniscal progenitors and the signaling pathways controlling their proliferation and differentiation. A greater understanding of the basic biology of meniscus-derived stem cells will be necessary for their application in cell based repair and tissue engineering strategies. To this end, we isolated and characterized meniscal stem progenitor cells (MSPCs) from adult mouse meniscus. We chose to analyze murine cells because our data could be used in future studies on the regulatory mechanisms underlying meniscal regeneration and the mouse is an ideal system for genetic manipulation. Mouse MSPCs exhibit the general features of tissue-specific stem cells isolated from other musculoskeletal tissues, including clonogenicity, multi-potency and expression of several common cell surface markers. In addition, adult mouse MSPCs express significant levels of genes first identified in embryonic mouse meniscus that may be important for meniscal formation. We also show that markers associated with MSPCs localize in distinct regions of the adult mouse meniscus hypothesized to harbor cells capable of responding to meniscal injury.

**METHODS:** This study was approved by the Harvard Medical School IACUC. MSPCs were isolated from C57Bl/6 mouse menisci grown in explant culture. These cells were characterized for stem cell properties using colony-forming assays and for their ability to differentiate in osteogenic, adipogenic and chondrogenic media. Flow cytometry was used to detect the presence of surface antigens related to stem cells on MSPC, and qRT-PCR was used to examine the gene expression profile of MSPCs. The major proteins associated with MSPCs were localized in the adult mouse knee using immunohistochemistry (IHC).

**RESULTS:** Based on explant culture procedures for human meniscus and cartilage, a protocol was developed for isolating meniscal progenitor cells from adult mouse meniscus. After 5-7 days, cells began to grow out of the explanted menisci (Figure 1A). In culture, these meniscus-derived cells grew clonally and exhibited a spindle-shaped morphology (Figure 1B). Cells grew out of both the lateral and medial menisci of mice of all ages tested (8wk, 6 mo, 1yr) and grew well in monolayer. Mouse MSPCs showed universal stem cell like characteristics including clonogenicity and multi-potentiality (Figure 1C-F). FACs analysis revealed MSPCs expressed the mesenchymal stem cell markers CD44, Sca-1, CD90 and CD73, and when cultured in monolayer had elevated levels of biglycan and collagen type I, important extracellular matrix components of adult meniscus. MSPCs also expressed robust levels of the meniscus signature gene *lysyl oxidase (Lox)*, an enzyme responsible for collagen cross-links in skeletal and connective tissue, as well as *Igf-1*, the major signaling pathway enriched in the developing meniscus. To verify data obtained from FACs and qPCR analyses with MSPC behavior *in vivo*, the spatial localization of a select group of MSPC expressed factors was examined using IHC. CD44, biglycan, Lox and IGF-1 were all detected in the outer periphery of the meniscus in the fibro-chondrocytes of the superficial zone of 8 wk old mice (Figure 2B-E). This superficial zone is thought to contain endogenous progenitor cells with regenerative capabilities. In addition, positive staining was seen for CD44, biglycan, Lox and IGF-1 in the fibroblast like cells of the outer vascular zone. This region is rich in collagen type I and has a higher capacity for healing and repair.

**DISCUSSION:** We believe that identification of MSPCs provides a powerful tool for enhancing cell-based strategies focused on meniscal regeneration, as there is increasing evidence that tissue-resident stem cells are critical for organ homeostasis and effective wound healing. Although MSCs and synovium-derived stem cells have been tested in meniscal injury models, endogenous stem/progenitor cells may be best suited for repair of the meniscus, a tissue with distinct composition, architecture and function in the knee joint.

**SIGNIFICANCE:** A greater understanding of the basic biology of meniscal stem/progenitor cells is needed to enhance treatments for meniscal pathologies. Analysis of meniscus derived-stem cells in animal models such as the mouse will allow for detailed studies of their behavior during injury and repair and of the regulatory pathways that guide these processes, critical steps in identifying therapeutic targets for the regeneration of diseased or injured meniscal tissue.

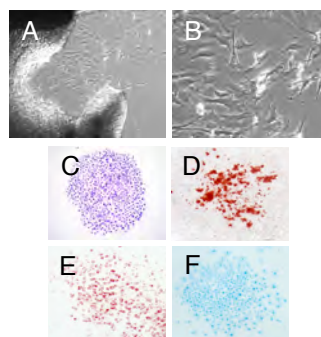


Figure 1. Isolation and analysis of MSPCs. (A) Cells growing out of lateral meniscus after 5 days in culture. (B) Spindle shaped morphology of these cells. (C) Sample colony formed by MSPCs stained with methyl violet. Multi-differentiation potential of MSPCs. (D) Alizarin Red S staining showing osteogenic differentiation. (E) Oil Red O staining showing adipogenic differentiation. (F) Alcian Blue staining showing chondrogenic differentiation.

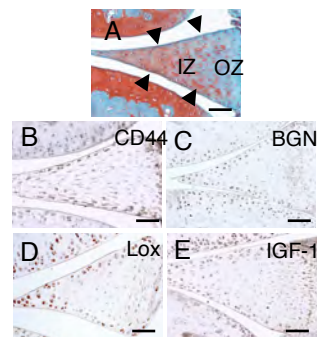


Figure 2. Localization of proteins associated with MSPCs in 8 wk mouse knee. (A) Safranin O of posterior meniscal horn. Arrowheads, superficial zone; IZ, inner zone; OZ, outer zone. IHC for (C) CD44 (D) Biglycan (E) Lox (F) IGF-1. Positive staining is detected in the superficial and outer zone of posterior horn of the meniscus. Scale bar = 100µm.

List of Personnel supported on this Project.

Vicki Rosen

Laura Gamer

Marina Feigenson

Steven Pregizer